Negative refraction of elastic waves on a metamaterial with anisotropic local resonance

Guy Bonnet, Vincent Monchiet

Negative refraction of elastic waves on a metamaterial with anisotropic local resonance

G. Bonnet[a,*], V. Monchiet[a]

[a] *Université Gustave Eiffel,Laboratoire Modélisation et Simulation Multi Echelle, MSME UMR 8208 CNRS, 5 bd Descartes, 77454 Marne-la-Vallée, France*

Abstract

Wave propagation through a locally resonant metamaterial characterized by anisotropic dynamic mass density is studied. The polarizations and velocities of waves are obtained from an extended Christoffel matrix. The set of waves induced by a body wave coming through the interface with an elastic material is described. Reflexion and refraction coefficients corresponding to the ratio of real Poynting vectors are obtained, showing that some of these coefficients are singular. In this case, the Poynting vector of the set of coupled waves must be used. This Poynting vector can display a negative refraction. The conditions leading to negative refraction are described and several examples of negative refraction are displayed.

Keywords: , Metamaterials, Elasticity, Resonance, Dynamic mass density, Negative refraction, Poynting vector, Exceptional point

1. Introduction

The works on metamaterials are numerous since the Veselago's paper (Veselago, 1968) on electromagnetism. In the case of acoustics, the concept of metamaterials was primarily used in the case "of materials using an (internal) structure much smaller than the sub-wavelength size" (Liu et al., 2020), the internal

*Corresponding author
Email address: guy.bonnet@u-pem.fr (G. Bonnet)
URL: www.msme.u-pem.fr (G. Bonnet)

structure having its own resonance frequency. These will be called in the following Metamaterials with Local Resonance (MLR) (Zhou et al., 2012; Ma & Sheng, 2016). This corresponds also to the concept of "inner resonance" (Boutin et al., 2018). However, with the success of the notion of metamaterials, numerous works are devoted to "metamaterials" having a periodic structure with moderate contrasts between the constituents of the material. In this case, the use of methods for multiscattering or of Bloch waves to study the overall behaviour is adequate and the "resonance" of the structure can not be related to a locally resonant internal structure, but to the collective response of the periodic structure. The term of "phononic crystal" is sometimes preferred to describe this kind of materials, but a significant amount of papers use also the term of metamaterial to name these structures. However, even if there are relationships between both kinds of behaviours, it is preferable to distinct these two classes of materials. We shall use in the following the term of Metamaterials with Collective Resonance (MCR) to call these latter materials. The main difference between MLR and MCR is that the effective constitutive equations of MLR are local in space and non-local in time (due to a frequency dependent behaviour of physical parameters), while effective constitutive equations for MCR are in most cases non-local in space and time, their effective constitutive equations being usually written by using wave-vectors (Willis, 1981; Nassar et al., 2015, 2016).

In the case of MLR, the inner resonators can be homogeneous inclusions, composite inclusions, beams, plates... Numerous papers in this field were published that either study the properties of metamaterials from a theoretical approach (Akl et al., 2012; Huang & Sun, 2011, 2012; Lee et al., 2009; Baz, 2010; Bigoni et al., 2013) or display experimentally the properties of such materials (Liu et al., 2000; Sheng et al., 2003; Naify et al., 2012; Yao et al., 2008; Park et al., 2012).

An important aspect of these works is that the dynamic behaviour exhibits an "effective dynamic mass density", that becomes negative at certain frequencies, as predicted or observed by several authors (Auriault & Bonnet, 1985; Au-

riault, 1994; Yao et al., 2008; Liu et al., 2000; Yang et al., 2008). The simplest way to produce MLR is to introduce locally "spring-mass resonators" that have resonance frequencies in the direction of the axis of the spring (Milton, 2007; Milton & Willis, 2007). For composites containing homogeneous inclusions or "composite inclusions", made of a massive inner core inside a soft coating, the dynamic density can be computed, after obtaining the internal field in inclusion at resonance and the resonance frequencies of the inclusion ((Auriault & Bonnet, 1985; Auriault & Boutin, 2012; Bonnet & Monchiet, 2015, 2017, 2020)). For spherical homogeneous or composite inclusions, the dynamic density is the same for any direction of the motion, but for cylindrical inclusions, the dynamic density has components that are not the same for a motion along the axis of the cylinder or in the transversal direction. The dynamic density is therefore anisotropic, more precisely transversally isotropic in this case. It is also possible to build structures with components of dynamic density being different along three different directions, as for composites with elliptic fibers (Bonnet & Monchiet, 2020). The anisotropy is also obtained in the case of a microstructure made of elastic beams or plates, as a reticulated body (Boutin et al., 2018). In this case, the anisotropy is basically obtained because the stiffness is higher for a motion along the direction of the beam than for a motion along the transversal direction. In this work, it will be considered that the metamaterial is characterized by an anisotropic dynamic density, at least transversally isotropic.

Since the first studies on metamaterials, it was suggested that some of these materials have the ability to induce a negative refraction of waves incident on the metamaterial. In the case of MLR, a negative refraction has been obtained for inclusions having not a rotational symmetry (Bigoni et al., 2013; Krushynska et al., 2017; Xie et al., 2013; Zhu et al., 2014). In the case of MCR, numerous cases of negative refraction have been obtained, most of them related to fluid waves (Brunet et al., 2015; Christensen & García De Abajo, 2012; Christiansen & Sigmund, 2016; Han et al., 2014; Hladky-Hennion et al., 2013; Kaina et al., 2015; Lemoult et al., 2013; Wu et al., 2017; Zhang & Liu, 2004). A case of interest is the case of MCR corresponding to stratified media (Srivastava, 2016;

Mokhtari et al., 2020; Willis, 2016). In this case, it is observed that the negative refraction is obtained when the layers of the material are perpendicular to the interface between the metamaterial and its interface with the ordinary material, but not in the other case. The present paper will show the occurrence of negative refraction at the interface with an anisotropic MLR, with a similar feature.

In section 2, the important aspects of dynamic mass density will be described. Section 3 will be devoted to the description of plane waves that appear in the case of anisotropic MLR. It will be considered that the overall elastic properties are isotropic, with a dynamic density being anisotropic. The plane waves will be described by using an "extended Christoffel matrix" as in anisotropic elasticity.

In section 4, the diffraction of elastic waves at the interface with a MLR will be studied and the method to obtain the transmission coefficients will be described. These transmission coefficients will be obtained from Poynting vectors computed from the incident elastic wave and from the refracted waves in the metamaterial.

Section 5 will be devoted to numerical applications in different cases of dynamic density and incident waves. Negative refraction will be shown to be related to the occurrence of a singularity of transmission coefficients. In section 6, the conditions to obtain negative refraction in terms of the parameters of the problem will be described.

2. Dynamic behaviour of metamaterials with local resonance and anisotropic dynamic density

The overall dynamic equation of a MLR in harmonic motion at radial frequency ω can be written as (Auriault & Bonnet, 1985; Auriault & Boutin, 2012):

$$\mathbf{div}(\mathbf{a}_{eff}.\boldsymbol{\epsilon}) + \omega^2 \boldsymbol{\rho}_{eff}(\omega).\mathbf{u} = 0 \tag{1}$$

where $\mathbf{u}$ is the displacement field, $\boldsymbol{\epsilon}$ the linearized strain tensor, $\mathbf{a}_{eff}$ is a constant effective elasticity tensor and $\boldsymbol{\rho}_{eff}(\omega)$ is a frequency dependent dynamic density. It is noteworthy that this dynamic equation is local in space,

but non-local in time, due to the frequency dependence of $\boldsymbol{\rho}_{eff}$.

The dynamic density $\boldsymbol{\rho}_{eff}(\omega)$ is a second order tensor, whose structure is a consequence of the geometry of the inclusions. Usually, the inclusions have defined planes of symmetry (spheres, cylinders, plates,...) and using these planes to define the coordinate axes produces a diagonal dynamic density characterized by its diagonal components $\rho_{ii}(\omega)$. The frequency dependence of the dynamic density comes from the resonance within the inclusions and can be built from the eigenfrequencies that are excited when the inclusions are moved by an overall acceleration along a given direction. For the first resonance frequency ω_{jr} related to direction j, the related component of dynamic density is given by:

$$\rho_{jj} = \rho_s + d\rho_j \frac{\omega^2}{\omega_{jr}^2 - \omega^2} \tag{2}$$

where ρ_s is the mass density at low frequencies ("static density"). ω_{jr} and $d\rho_j$ are the resonance frequency and the part of mass density contributing to the dynamic density for a motion along direction j.

Introducing $\omega^* = \omega/\omega_{2r}$ and $d\rho^* = \frac{d\rho_2}{\rho_s}$, the expression of ρ_{22} is given by:

$$\rho_{22} = \rho_s(1 + d\rho^* \frac{\omega^{*2}}{1 - \omega^{*2}}) \tag{3}$$

Figure 18 displays $\frac{\rho_{22}}{\rho_s}$ as a function of ω^* for a given value of $d\rho^* = \frac{d\rho_2}{\rho_s}$. It shows that ρ_{22} can be negative above the resonance frequency up to $\omega^* = \sqrt{1/(1 - d\rho^*)}$.

For an anisotropic density being at least transversally isotropic, there are at least two different eigenfrequencies corresponding to the motions along two different directions of motion, i.e. $\rho_{11} \neq \rho_{22}$ and $\omega_{1r} \neq \omega_{2r}$. If $\omega_{2r} < \omega_{1r}$ and if the difference between these eigenfrequencies is large enough, one can consider that $\rho_{11} \sim \rho_s$ when ρ_{22} becomes negative. As an example, the metamaterial made of composite cylindrical fibers containing internal fibers inside a soft coating was studied in Bonnet & Monchiet (2015). The lowest eigenfrequency corresponds to a motion in the direction of the fibers. The ratio between this eigenfrequency and the one related to a motion transversal to the fibers depends on the Poisson's ratio. For a Poisson's ratio of 0.42, the ratio between the eigenfrequencies

is 2. The component of dynamic density related to the second eigenfrequency corresponds to $\omega/\omega_r = 0.5$. It can be seen from figure 18 that the related component of dynamic mass density is nearly equal to ρ_s.

The lowest resonance frequency of inclusions depends on their orientation. Changing this orientation allows us to choose the direction related to the lowest resonance frequency. In the following, the first resonance will be related to a motion along either x_1 or x_2. For studying the refraction of waves in section 3, the value of $d\rho^*$ will be chosen equal to 0.3 and the frequency of incident waves will be chosen initially at the center of frequency range of negative dynamic density, leading to $\rho_{22} \sim -0.765\rho_s$.

3. Extended Christoffel matrix for locally resonant metamaterials with an anisotropic dynamic density

As explained in section 2, dynamic density is characterized by eigenfrequencies of inclusions and some among its components can become negative near eigenfrequencies. The main goal of this work is to study the effect of such negative dynamic density components on the propagation of elastic waves and on the scattering of waves at the interface between an elastic material and a metamaterial, specifically in the case of an anisotropic dynamic density.

The resonators contained in the MLR having an anisotropic dynamic density, this induces generally an anisotropy of effective elastic properties, as for example in the case of cylindrical inclusions. However, it is possible to conceive composite inclusions having an anisotropic dynamic density, the overall material being elastically isotropic. This is the case if the elastic anisotropy of the resonators has a negligible effect on the anisotropy of the overall elasticity tensor. A typical example is the case of a metamaterial made of a random distribution of spherical inclusions containing resonating beams. The beams can be conceived to have a negligible effect on the global elasticity tensor and lead to an overall anisotropic dynamic density if they are all oriented along the same direction.

Studying this case will allow us to simplify the scattering problem in the

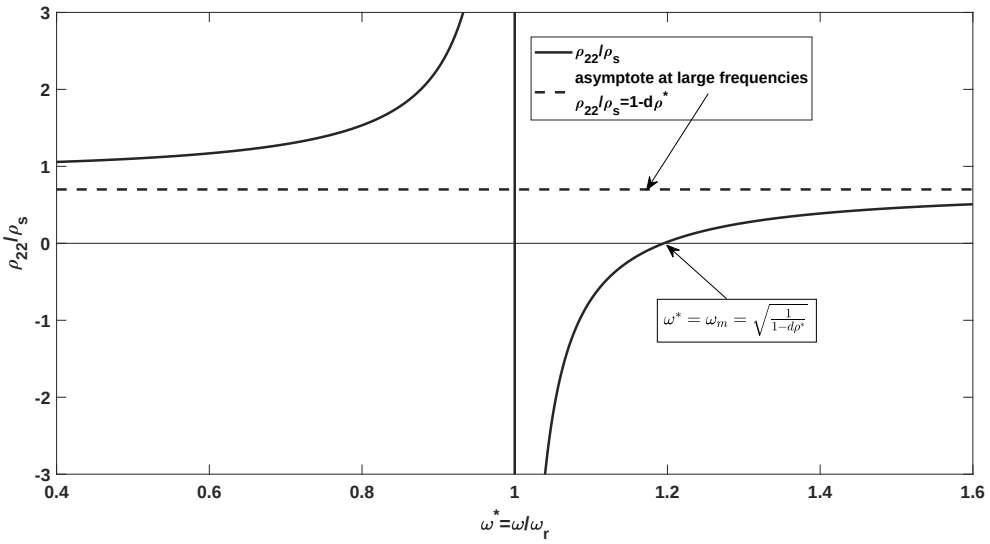

Figure 1: Dynamic density as a function of the non-dimensional frequency

following section, while keeping the main features of the physical problem : propagation and refraction related to a metamaterial of anisotropic density. Then, the overall dynamic equation for an harmonic motion of the metamaterial becomes:

$$\mu \Delta u_i + (\lambda + \mu) \frac{\partial^2 u_j}{\partial x_i \partial x_j} + \omega^2 \rho_{ij} u_i = 0 \tag{4}$$

where $\rho_{ij} = \delta_{ij} \rho_{jj}(\omega)$ are the components of the diagonal dynamic density at a given frequency ω, λ and μ being Lamé coefficients.

Looking for plane waves propagating in the direction of $\mathbf{p}$ (components p_i) with a wave velocity v leads to:

$$\Gamma_{ij} u_j = \mu u_i + (\lambda + \mu) p_i . p_j u_j = v^2 \rho_{ii} u_i \tag{5}$$

The components Γ_{ij} are those of the Christoffel matrix [Γ] (Auld, 1973) in the

particular case of an isotropic elasticity tensor.

This system can be written as:

$$[\Gamma]\begin{bmatrix} u_1 \\ u_2 \\ u_3 \end{bmatrix} = v^2.\begin{bmatrix} \rho_{11} & 0 & 0 \\ 0 & \rho_{22} & 0 \\ 0 & 0 & \rho_{33} \end{bmatrix}.\begin{bmatrix} u_1 \\ u_2 \\ u_3 \end{bmatrix} = v^2[\rho]\begin{bmatrix} u_1 \\ u_2 \\ u_3 \end{bmatrix} \tag{6}$$

For an isotropic density, the matrix $[\rho]$ is diagonal, with $\rho_{ii} = \rho$ and the eigenvalues of $[\Gamma]$ are equal to $\lambda_i = \rho.v_i^2$, producing the wave velocities v_i.

For an anisotropic density, equation (6) shows that v_i^2 are the generalized eigenvalues of the couple $([\Gamma], [\rho])$, these two matrices being symmetrical. However, when all diagonal values of $[\rho]$ are not null, it is easier to write:

$$[\rho]^{-1}.[\Gamma] = [\Upsilon]\begin{bmatrix} u_1 \\ u_2 \\ u_3 \end{bmatrix} = v^2\begin{bmatrix} u_1 \\ u_2 \\ u_3 \end{bmatrix} \tag{7}$$

Thus, the wave velocities are given more easily by the eigenvalues of $[\Upsilon]$ and the wave motion of plane waves by its eigenvectors, similarly to the usual Christoffel matrix. So, $[\Upsilon]$ can be considered as an "extended Christoffel matrix". However, this matrix is the product of two matrices that do not diagonalize in the same base and is therefore not symmetric. For a plane wave propagation in plane (x_1, x_2), the components of the extended Christoffel matrix are given by:

$$[\Upsilon] = \begin{bmatrix} \frac{\mu}{\rho_{11}} + (\lambda+\mu)\frac{p_1.p_1}{\rho_{11}} & (\lambda+\mu)\frac{p_1.p_2}{\rho_{11}} & 0 \\ (\lambda+\mu)\frac{p_1.p_2}{\rho_{22}} & \frac{\mu}{\rho_{22}} + (\lambda+\mu)\frac{p_2.p_2}{\rho_{22}} & 0 \\ 0 & 0 & \frac{\mu}{\rho_{33}} \end{bmatrix} \tag{8}$$

It is noteworthy that $[\Upsilon]$ is no more symmetric contrarily to the case of the usual Christoffel matrix which is always symmetric, even in the case of anisotropic elasticity tensors with isotropic mass density.

3.1. SH waves

The unit vector $\mathbf{e}_3$ in the direction of Ox_3 is an obvious eigenvector and therefore a direction of polarization. It corresponds to shear waves whose po-

larization is perpendicular to the plane x_1x_2, i.e. SH waves, according to an usual appellation. These waves differ from usual elastic waves only in the case where ρ_{33} becomes negative, the waves becoming evanescent for any direction of propagation.

3.2. Waves with a polarization in a plane containing the direction of propagation

In the case of a polarization in the plane x_1x_2, the wave velocities and polarizations are obtained from the diagonalization of the upper (2×2) matrix. Denoting θ the angle between the unit vector direction $\mathbf{p}$ in the direction of propagation and direction Ox_2, the related system can be written as:

$$F\left[\Upsilon_0\right] \begin{bmatrix} u_1 \\ u_2 \end{bmatrix} = v^2 \begin{bmatrix} u_1 \\ u_2 \end{bmatrix} \tag{9}$$

where

$$[\Upsilon_0] = \begin{bmatrix} b - \cos 2\theta & \sin 2\theta \\ a \sin 2\theta & a(b + \cos 2\theta) \end{bmatrix} \tag{10}$$

and $a = \rho_{11}/\rho_{22}$, $b = (\lambda + 3\mu)/(\lambda + \mu) = 3 - 4\nu$ and $F = (\lambda + \mu)/(2\rho_{11})$. For a material with static mass density ρ_s and compressional wave velocity $\alpha = \sqrt{\frac{\lambda+2\mu}{\rho_s}}$, F is given by:

$$F = \frac{\alpha^2}{4(1-\nu)} \frac{\rho_s}{\rho_{11}} \tag{11}$$

The wave velocities v_1, v_2 for a direction of propagation related to θ are given by $v_{1,2}^2 = F.r_{1,2}$ where $r_{1,2}$ are the solutions of

$$r^2 - Tr + P = 0 \tag{12}$$

with

$$\begin{aligned} T &= tr([\Upsilon_0]) = (b(1+a) + \cos 2\theta(a-1)) \\ P &= \det([\Upsilon_0]) = a(b^2 - 1) \end{aligned} \tag{13}$$

It can be shown that for any angle θ real , the values of r are real. The product of the squares of the wave velocities is given by

$$v_1^2 v_2^2 = \frac{(\lambda + 2\mu)\mu}{\rho_{11}\rho_{22}} \tag{14}$$

This is consistent with the usual values obtained for P-waves (α) and S-Waves (β) in the case of an isotropic behaviour , $\beta^2 = \mu/\rho_s, \alpha^2 = (\lambda + 2\mu)/\rho_s$

From the expressions above:

- If both ρ_{11} and ρ_{22} are positive and real , v_1 and v_2 are real.
- If ρ_{11} and ρ_{22} are of opposite sign, one of the wave velocities is real and the other is purely imaginary.
- If both ρ_{11} and ρ_{22} are negative and real, it can be shown that the solutions for equation (12) are both positive. However F is negative, leading to two purely imaginary wave velocities.

3.3. Polarization of waves within plane x_1x_2

For the waves polarized in plane x_1x_2, the components of the polarization vector are given by the eigenvectors $\mathbf{k}, \mathbf{l}$ of Υ_0. The components of the eigenvector $\mathbf{k}$ (or similarly for $\mathbf{l}$) associated with one value of r are therefore given by:

$$\begin{aligned} k_1 &= \frac{\sin 2\theta}{N} \\ k_2 &= \frac{r - b + \cos 2\theta}{N} \\ N^2 &= \sin^2 2\theta + (r - b + \cos 2\theta)^2 = (r - b)^2 + 2(r - b)\cos 2\theta + 1 \end{aligned} \tag{15}$$

The scalar product of the two polarization vectors is:

$$\mathbf{k}.\mathbf{l} = \sin^2 2\theta(a - 1) \tag{16}$$

These vectors are not orthogonal except if the material is isotropic ($a = 1$) or if the direction of propagation is parallel to one of the axes ($\sin 2\theta = 0$).

3.4. Waves within a metamaterial having an anisotropic dynamic density

We consider that the MLR is such that $\rho_{11} = \rho_s$ and ρ_{22} depends on the frequency as described in the previous section.

The value of the dynamic part of mass density is given by $d\rho^* = 0.3$ and the ratio of densities a is given by:

$$a = \frac{1 - \omega^{*2}}{1 + (d\rho^* - 1)\omega^{*2}} \tag{17}$$

3.4.1. Frequency dependence of selected waves

In a first step we look at the effect of the frequency dependence of ρ_{22} on wave propagation.

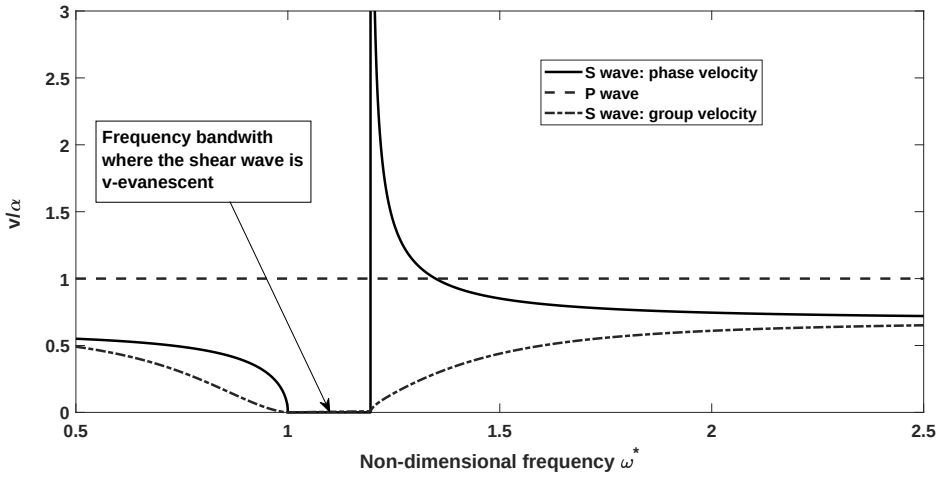

Figure 2: Wave velocities for a direction of propagation along x_1.The figure displays the bandgap where the shear wave is v-evanescent, because the wave velocity is purely imaginary.

Figure 2 shows the frequency dependence of the wave velocities for a direction of propagation along Ox_1. The results are consistent with the nature of the

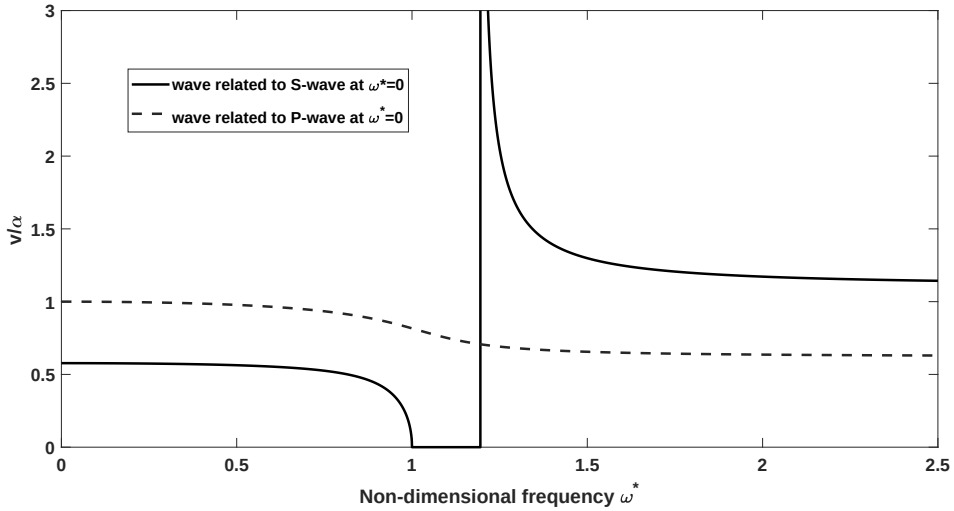

Figure 3: Wave velocities (phase velocities) for a direction of propagation at an angle of $\pi/4$ with respect to x_2.

dynamic density. The motion along Ox_1 is characterized by a static density, leading to the compressional wave velocity for any frequency. On the contrary, the shear wave is not propagating within the bandgap $1 < \omega^* < \omega_m$, where ω_m corresponds to the change of sign of ρ_{22}, given by: $\omega_m = \sqrt{\frac{1}{1-d\rho^*}}$. Within this bandgap, the shear wave becomes evanescent, as shown in appendix D. Due to the fact that the structure of the wave is different from the classical evanescent waves in classical elasticity theory, the wave is named "v-evanescent".

At frequency ω_m, the dynamic density vanishes. As a consequence, the phase velocity tends to infinity. However, in this case, due to the dispersion, the phase velocity is strongly different from the group velocity, computed by the relation given in appendix B, as it can be seen on the figure. The polarization of waves are the same as in the usual case.

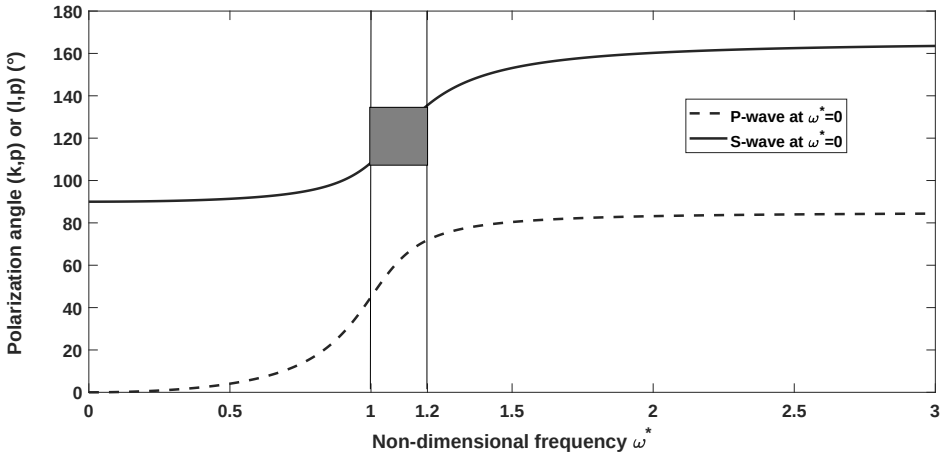

Figure 4: Direction of polarization of waves with respect to the direction of propagation for waves propagating at an angle of $\pi/4$.

Figure 3 shows the frequency dependence of wave velocities for a direction of propagation at $\theta = \pi/4$. The situation is clearly different from the previous one. There are two waves: one is always propagating. It corresponds to the P wave at low frequency. However, this wave is now dispersive, with a variation of the phase velocity. The second wave corresponds to shear wave at low frequency. It is characterized by a bandgap in the same frequency range as in the previous case, where the wave is v-evanescent. The asymptotic values of the wave velocities for $\omega^* \gg \omega_r$ can be obtained, leading to $v_1 = 1.11\alpha$ and $v_2 = 0.62\alpha$. Both values are higher than the velocities at low frequency. This is due principally to the fact that $\rho_{22} = \rho_s(1 - d\rho^*) < \rho_s$ for large frequencies, leading to higher wave velocities. In addition, the material does not recover the isotropy of mass density, due to the fact that $\rho_{22} < \rho_s$ at high frequency.

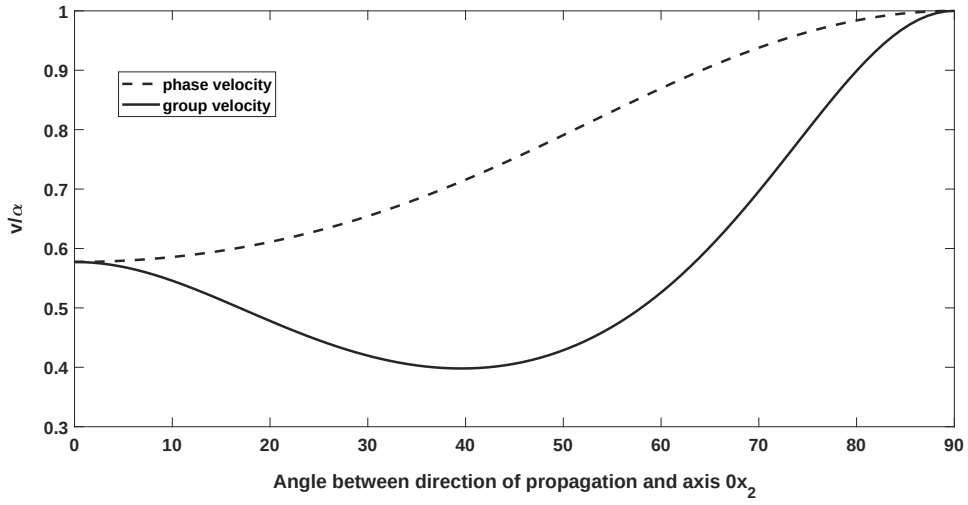

Figure 5: Wave velocity of the propagating wave at the center of frequency range of negative dynamic density ρ_{22}. Variation of phase velocity and group velocity as a function of the angle between Ox_2 and the direction of propagation.

In this case, the polarization of waves is no more transversal or longitudinal as soon as the mass density anisotropy becomes significant. Figure 4 shows the variation of the angle $\phi = (\mathbf{p}, \mathbf{k})$ (or $(\mathbf{p}, \mathbf{l})$) between the direction of polarization and the direction of propagation for both waves. It can be seen that at low frequency, the polarizations are oriented at $\phi = O$ for P-waves and $\pi/2$ for S-waves. Within the frequency bandgap, the wave corresponding to P wave at low frequency has a direction of polarization oriented at $\pi/4$ at resonance $\omega^* = 1$, i.e. along $0x_1$ and the angle $(\mathbf{p}, \mathbf{k})$ increases within the bandgap. It means that the wave is no more compressional. As previously, the asymptotic values of the polarization angles can also be obtained, leading to 85 and 165.5 degrees. It means that the waves do not recover the nature of S-waves and P-waves,

due to the persistent anisotropy of dynamic mass density above the resonance frequency.

3.4.2. Dependence of wave velocity with angle of propagation

Figure 5 displays the variation of phase velocity and group velocity of propagating waves for different directions of wave propagation, at the center of negative mass density range. The figure shows that the phase velocity increases continuously from S-wave velocity to P-wave velocity. The difference between phase velocity and group velocity is significant and is maximum for $\theta = \pi/4$, the group wave velocity being equal to nearly half the phase wave velocity. It is noticeable that the group velocity and phase velocity are equal for angles of propagation 0 and $\pi/2$. In this case, the propagating waves are polarized as usual S-waves or P-waves being independent from the frequency.

4. Refraction of waves at the interface between an elastic material and a metamaterial.

In the previous section it has been shown that the anisotropy of mass density of a locally resonant material leads to a strongly modified scheme of wave propagation. In this section, the consequences on the reflected/refracted waves at the interface between an elastic material and a metamaterial are studied.

4.1. The waves fields pattern at the interface between an elastic medium and a locally resonant metamaterial.

One considers an incident elastic wave on a plane interface coming from an elastic material. This one will be considered as the superposition of incident P and S-waves (displacement $\mathbf{u}_{ip}$ and $\mathbf{u}_{is}$), with

$$\mathbf{u}_{ip} = A_{ip}\mathbf{s}(\sin i_1, \cos i_1) \exp\left[i\omega\left(px_1 + \frac{\cos i_1}{\alpha_1}x_2 - t\right)\right] \tag{18}$$

and

$$\mathbf{u}_{is} = A_{is}\mathbf{s}(\cos j_1, -\sin j_1) \exp\left[i\omega\left(px_1 + \frac{\cos j_1}{\beta_1}x_2 - t\right)\right] \tag{19}$$

where α_1, β_1 are the P and S wave velocities in medium 1 and $\mathbf{s}(s_1, s_2)$ denotes the polarization vector of the wave, i.e. the unit vector of components s_1, s_2. A_{is} and A_{ip} are the amplitudes of the waves. p is the horizontal slowness, whose continuity must be ensured at the interface and i_1, j_1 are the incidence angles, i.e. the angles between the directions of incidence and axis x_2.

The reflected waves are:

$$\begin{aligned} \mathbf{u}_{rp} &= A_{rp}\mathbf{s}(\sin i_1, -\cos i_1) \exp\left[i\omega\left(px_1 - \frac{\cos i_1}{\alpha_1}x_2 - t\right)\right] \\ \mathbf{u}_{rs} &= A_{rs}\mathbf{s}(\cos j_1, \sin j_1) \exp\left[i\omega\left(px_1 - \frac{\cos j_1}{\beta_1}x_2 - t\right)\right] \end{aligned} \tag{20}$$

and the waves transmitted through the metamaterial are:

$$\begin{aligned} \mathbf{u}_f &= A_f\mathbf{f} \exp\left[i\omega\left(px_1 + \frac{\cos\theta_f}{v_f}x_2 - t\right)\right] \\ \mathbf{u}_g &= A_g\mathbf{g} \exp\left[i\omega\left(px_1 + \frac{\cos\theta_g}{v_g}x_2 - t\right)\right] \end{aligned} \tag{21}$$

where $\mathbf{f}, \mathbf{g}$ are the polarization vectors of waves through the metamaterial, as defined in the previous section. v_f and v_g are the corresponding wave velocities and θ_f, θ_g define the directions of propagation through the metamaterial. The notations for the polarizations are changed from section 3 where $\mathbf{k}, \mathbf{l}$ were the polarizations of waves propagating in the same direction. Now, transmitted waves (refracted waves) through the interface have no more the same direction of propagation, because the direction of propagation must be compatible with the horizontal slowness of the incident wave, as shown in the following subsection.

4.2. Computation of the refraction angles and wave velocities within the metamaterial.

The angles of reflection and refraction are obtained directly from the incidence angles by the continuity of the horizontal slowness:

$$\frac{\sin i_1}{\alpha_1} \left(\text{or } \frac{\sin j_1}{\beta_1}\right) = p \tag{22}$$

This relation can be also written for the metamaterial:

$$\frac{\sin\theta_f}{v_f} = \frac{\sin\theta_g}{v_g} = p \tag{23}$$

v_f and v_g are related to r, solutions of (12) by $v^2 = F.r$ and θ_f, θ_g correspond to θ in the notation of the previous section. This leads to:

$$v^2 = \frac{\sin^2\theta}{p^2} = Fr \tag{24}$$

and therefore:

$$r = \frac{(1-\cos 2\theta)}{2Fp^2}, \tag{25}$$

leading to:

$$\cos 2\theta = 1 - 2rFp^2 \tag{26}$$

but from equation (12), r is also solution of $r^2 - Tr + P = 0$ where $T = H + L\cos 2\theta$, denoting $H = b(1+a), L = a - 1$. This leads to:

$$r^2 - (H + L\cos 2\theta)r + P = 0 \tag{27}$$

replacing $\cos 2\theta$ by its expression (26) leads to:

$$(1 + 2FLp^2)r^2 - (H + L)r + P = 0 \tag{28}$$

This equation produces the values of r that are compatible with the horizontal slowness p. The related wave velocities v_f, v_g are obtained from $v^2 = Fr$ and the related angles θ_f, θ_g are obtained from the value of θ given by $sin(\theta_{f,g}) = p.v_{f,g}$. As it will be shown thereafter, equation (28) contains the major part of information characterizing the pattern of refracted waves.

4.2.1. Refracted waves for ρ_{11} negative.

The refracted waves given by equation (28) can be evanescent or propagative according to the sign of r and to the nature of θ. A first case of interest is when $\rho_{11} < 0$ and $\rho_{22} > 0$. In this case, the parameters are such that $a < 0, L < 0, P < 0, F < 0$. As a consequence, equation (28) has two real solutions of opposite sign. It means that one of the values of v is real and the other purely

imaginary. The second wave, related to $r > 0$ is always evanescent (because $F < 0$ leading to $v^2 < 0$). The angle of refraction of the evanescent wave is imaginary because $cos2\theta > 1$. For the value $r < 0$, the wave is propagative if θ is real. This is achieved if $sin\theta = p.v < 1$ where v is the wave velocity of the propagating wave, i.e. for velocities below the limit corresponding to the grazing refraction, as in classical elasticity theory.

4.2.2. Scattered waves for ρ_{22} negative.

The parameters are such that $a < 0, L < 0, P < 0, F > 0$ When $\rho_{22} < 0$ and $\rho_{11} > 0$, the properties of waves through the metamaterial are obtained from the signs of $L + H$ and $1 + 2FLp^2$.

With $P < 0$, the roots of equation (28) are of opposite sign if $1+2FLp^2 > 0$. In this case, there is again only one real wave velocity corresponding to $r > 0$. This wave is propagative again under the condition $sin(\theta) < 1$.

If $1 + 2FLp^2 < 0$, the roots of the equation are both of the same sign. They are real if the discriminant of the equation is >0, i.e. $(L+H)^2-4P((1+2FLp^2) > 0$ and related to a real wave velocity if $L + H < 0$ (two positive roots). In this case, there are zero, one or two propagative waves, depending on $sin(\theta_f)$ (or $sin(\theta_g)$) being lower or higher than 1.

4.3. Equations of continuity at the interface.

The reflected and transmitted waves are obtained from the continuity of the displacement and traction at the interface. The equations on the elastic side are detailed in classical books (Auld, 1973; Eringen & Suhubi, 1978) and the equations on the metamaterial side are obtained from the derivation of the displacement field, leading to :

$$[M_1] \begin{bmatrix} A_{ip} \\ A_{is} \\ A_{rp} \\ A_{rs} \end{bmatrix} = [M_2] \begin{bmatrix} A_f \\ A_g \end{bmatrix} \tag{29}$$

where $[M_1]$ and $[M_2]$ are given by:

$$[M_1] = \begin{bmatrix} \sin i_1 & \cos j_1 & \sin i_1 & \cos j_1 \\ \cos i_1 & -\sin j1 & -\cos i_1 & \sin j_1 \\ \rho_1\alpha_1(1-2\beta_1^2p^2) & -2\rho_1\beta_1^2p\cos j_1 & \rho_1\alpha_1(1-2\beta_1^2p^2) & -2\rho_1\beta_1^2p\cos j_1 \\ 2\rho_1\beta_1^2p\cos i_1 & \rho_1\beta_1(1-2\beta_1^2p^2) & -2\rho_1\beta_1^2p\cos i_1 & -\rho_1\beta_1(1-2\beta_1^2p^2) \end{bmatrix}$$

and

$$[M_2] = \begin{bmatrix} f_1 & g_1 \\ f_2 & g_2 \\ \lambda_2 p f_1 + \frac{(\lambda_2+2\mu_2)}{v_f} f_2 \cos\theta_f & \lambda_2 p g_1 + \frac{(\lambda_2+2\mu_2)}{v_g} g_2 \cos\theta_g \\ \mu_2\left(\frac{f_1}{v_f}\cos\theta_f + p f_2\right) & \mu_2\left(\frac{g_1}{v_g}\cos\theta_g + p g_2\right) \end{bmatrix} \tag{30}$$

where λ_2 and μ_2 are the Lamé coefficients of the metamaterial and ρ_1 is the mass density of the elastic material. The two first lines of (29) come from the continuity of displacement and the two last ones from the continuity of traction at the interface. This can be written :

$$\begin{aligned} [M_{1A}] \begin{bmatrix} A_{ip} \\ A_{is} \end{bmatrix} &= -[M_{1B}] \begin{bmatrix} A_{rp} \\ A_{rs} \end{bmatrix} + [M_2] \begin{bmatrix} A_f \\ A_g \end{bmatrix} \\ &= [T] \begin{bmatrix} A_{rp} \\ A_{rs} \\ A_f \\ A_g \end{bmatrix} \end{aligned} \tag{31}$$

where $[M_{1A}]$ contains the first two columns of $[M_1]$ and $[M_{1B}]$ the other ones.

Finally, the unknown coefficients are given by:

$$\begin{bmatrix} A_{rp} \\ A_{rs} \\ A_f \\ A_g \end{bmatrix} = [T]^{-1}[M_{1A}] \begin{bmatrix} A_{ip} \\ A_{is} \end{bmatrix} \tag{32}$$

The first column of the matrix $[T]^{-1}[M_{1A}]$ gives the reflexion and transmission coefficients for an incident P-wave and the second one produces those related to an incident S-wave.

4.4. Poynting vector

The flow of energy transmitted by the plane waves can be computed by using the Poynting vector which is the time average of the product of the stress tensor by the velocity. In complex notation, the Poynting vector is given by the real part of the complex Poynting vector (Auld, 1973) obtained from:

$$\mathbf{P} = -\frac{1}{2}\boldsymbol{\sigma}.\boldsymbol{v}^* \tag{33}$$

where $\boldsymbol{\sigma}$ contains the complex components of the stress tensor and $\mathbf{v}^*$ is the conjugate of the complex velocity.

For a wave within the metamaterial with a polarisation $\mathbf{f}$ and with a propagation vector $\mathbf{p}$, the related Poynting vector is given by:

$$\mathbf{P}_f = \frac{|A_f|^2 \omega^2}{2v_f} \left[\boldsymbol{\Sigma}_f\right].\mathbf{f}^* \tag{34}$$

where

$$\boldsymbol{\Sigma}_f \quad = \quad \mu\left[\mathbf{f}\otimes\mathbf{p} + (\mathbf{f}\otimes\mathbf{p})^T\right] + \lambda\left(\mathbf{f}.\mathbf{p}\right)\mathbf{I}$$

This expression leads to the usual expressions of Poynting vectors in the case of S and P waves. The transmission coefficients are obtained by the ratio of the modulus of the real part of Poynting vector divided by the modulus of the real part of Poynting vector of the incident wave, leading to:

$$\chi_f = \frac{1}{\rho_i.v_i}\left|\frac{A_f}{A_i}\right|^2 |Re\left(\frac{1}{v_f}\left[\boldsymbol{\Sigma}_f\right].\mathbf{f}^*\right)| \tag{35}$$

where ρ_i, v_i are the mass density and wave velocity of the incident wave.

This expression has been obtained for an harmonic wave. However, it has been shown in section 2 that the propagating waves are dispersive, due to the frequency dependence of phase wave velocity. Therefore, the computation of energy flux should account for the dispersion. In appendix C, it is shown that the effect of dispersion on the time average Poynting vector can be neglected in the case of a wave train containing a large amount of oscillations at frequency ω. This will be assumed in the following.

5. Numerical application

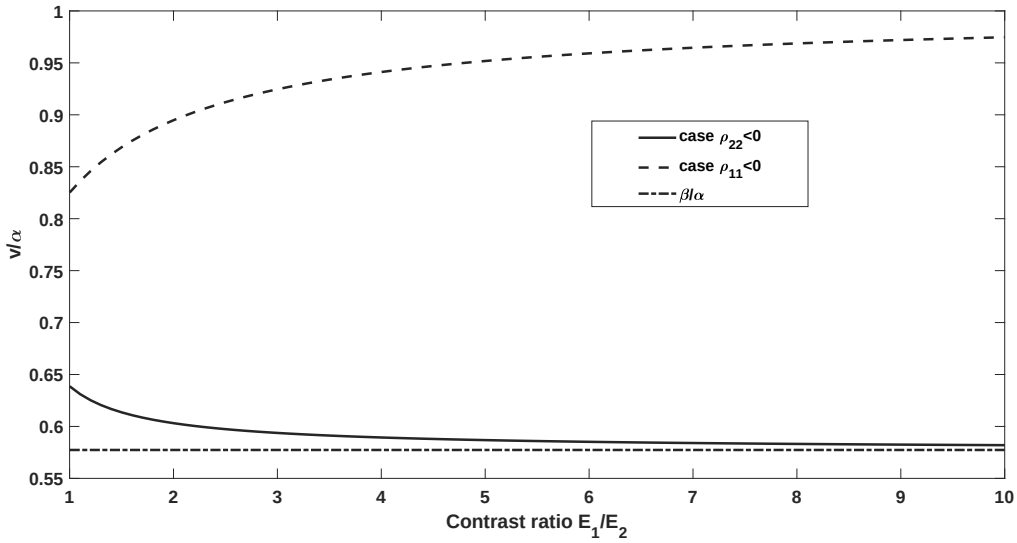

Figure 6: Wave velocities of the transmitted wave for each of the two cases $\rho_{22} < 0$ and $\rho_{11} < 0$. Case of a P-wave incident at $\pi/4$ on the interface.

We will consider the case of a direction of propagation in the plane x_1, x_2 when the Poisson's ratio of the metamaterial at low frequencies is the same as the one of the elastic material. The physics of the refraction within the interface is obviously governed by the nature of the dynamic density whose frequency dependence has been studied in section 2. In the case of two negative components of the dynamic density, the transmitted waves are both v-evanescent without penetration into the metamaterial. Therefore, in this section, we shall consider that one of the components of dynamic density is negative, the frequency being chosen at the center of the frequency bandwith of the related component of negative density.

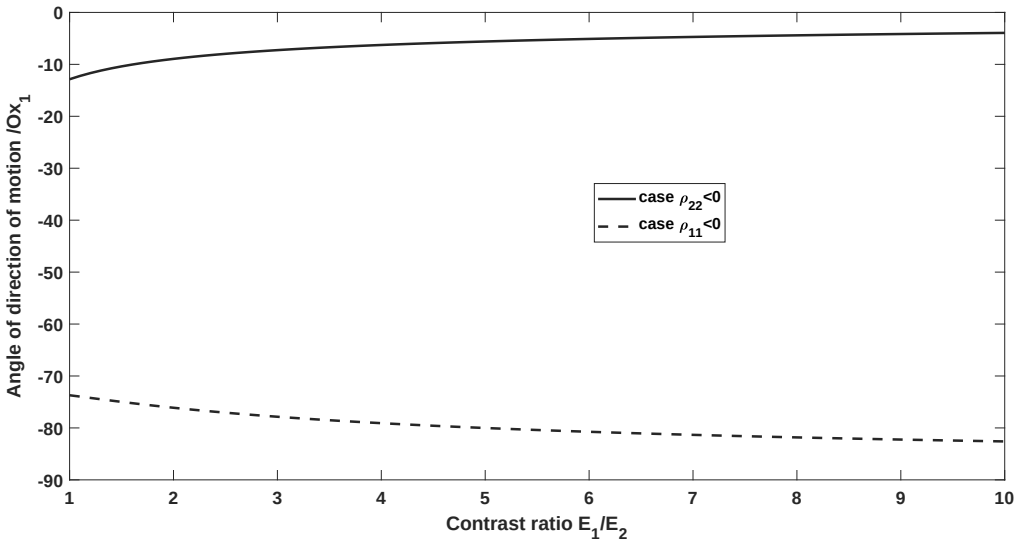

Figure 7: Angle of the direction of the polarization vector of the transmitted wave with respect to x_1 (two cases of dynamic density). Case of a P-wave incident at $\pi/4$ on the interface.

As in section 2, we consider a metamaterial such that the ratio of the resonant mass density to the total mass density is equal to $d\rho^* = 0.3$. The negative density at the center of negative frequency bandwith is $\rho_{cent} = -0.765\rho_s$. The elastic medium and the metamaterial have the same Poisson's ratio $\nu = 1/4$ and the contrast of elastic properties, defined by the ratio $E_0 = E_1/E_2$ of the elastic moduli is variable.

The anisotropic density is characterized by the fact that one of the components of the dynamic density is negative, the other one being positive. We consider therefore the two cases $\rho_{22} = \rho_{cent} < 0, \rho_{11} = \rho_s$ and $\rho_{11} = \rho_{cent} < 0, \rho_{22} = \rho_s$.

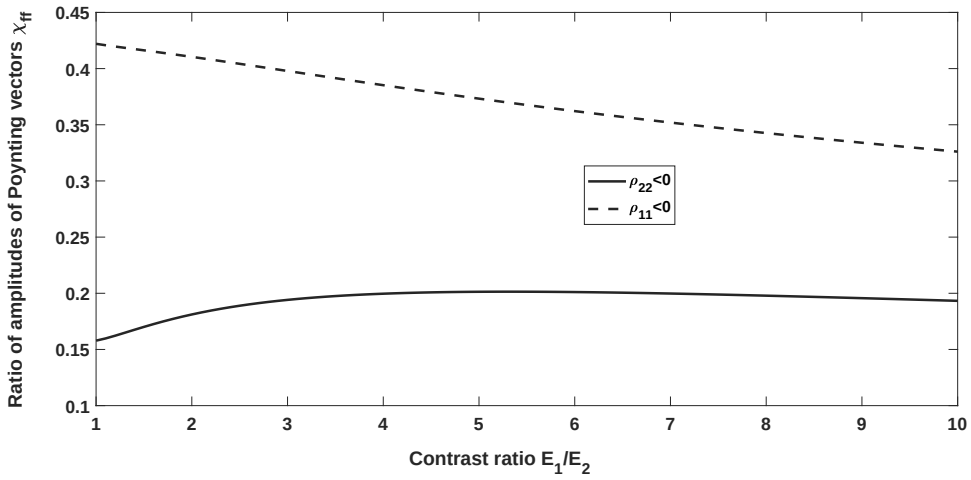

Figure 8: Ratio of the amplitudes of Poynting vectors between incident and transmitted wave. Case of a P-wave incident at $\pi/4$ on the interface.

5.1. Refraction-reflexion of incident P-waves.

5.1.1. Wave-velocities of transmitted waves

The case of a P-wave incident on the interface between both materials is studied, with an angle of incidence of $\pi/4$, the waves coming from the elastic material with a variable Young's modulus being higher than the one of the metamaterial. In a first step, the values of wave-velocities obtained for both cases are displayed on Fig. 6. In both cases, there is only one transmitted propagating wave, the other one being v-evanescent. In the case $\rho_{22} < 0$, it can be seen that the wave velocity of the transmitted wave is approximately 0.64 times the value of the velocity of the P-wave, and decreases towards the one of S-wave for increasing contrasts. Indeed, the negative value of $\rho_{22} < 0$ results in

a damping of the component u_2, the wave being characterized by a predominant value of u_1. For the case $\rho_{11} < 0$, the inverse effect is obtained and the wave velocity tends toward the one of P-waves at large contrasts.

5.1.2. Polarization of transmitted waves

In Fig. 7, the angle between the polarization vector and axis x_1 is displayed. It can be seen that the effect of damping of the motion along x_2 produces a motion nearer to axis x_1 for $\rho_{22} < 0$, with a smaller angle for increasing values of the contrast ratio. A similar effect is obtained for $\rho_{11} < 0$, but with a motion nearing instead the direction of x_2 at large contrasts.

5.1.3. Transmission coefficients.

Fig. 8 displays the ratio of the amplitudes of Poynting vectors obtained in the two cases of negative values of one component of dynamic density. In the case of $\rho_{22} < 0$, the ratio of amplitudes is small, being comprised between 0.16 and 0.19, with a maximum being around $E_0 = E_1/E_2 = 5$. For $\rho_{11} < 0$, the energy of transmitted wave is higher, between 0.32 and 0.38. It can be explained by the fact that in the first case, the wave is "nearly S-wave", while in the second case, the transmitted wave is "'nearly P-wave"', leading to a higher value of transmission coefficient, from equation (35).

These results are obtained when $E_1 > E_2$. In this case, there is always only one propagating wave. For $E_1 < E_2$, the refraction would be different, with possible occurence of two evanescent waves or two propagating waves, as in the case of incident S waves This is not studied here.

5.2. Refraction-reflexion of incident S-waves

5.2.1. Wave velocities of transmitted waves

In this case, the wave coming from the elastic material is a S-wave with an incidence of $\pi/4$. The velocities of waves transmitted through the metamaterial are displayed on Fig. 9. In the case of $\rho_{22} < 0$, the wave velocities v_f and v_g of transmitted wave are complex with a non-zero real part for a contrast ratio

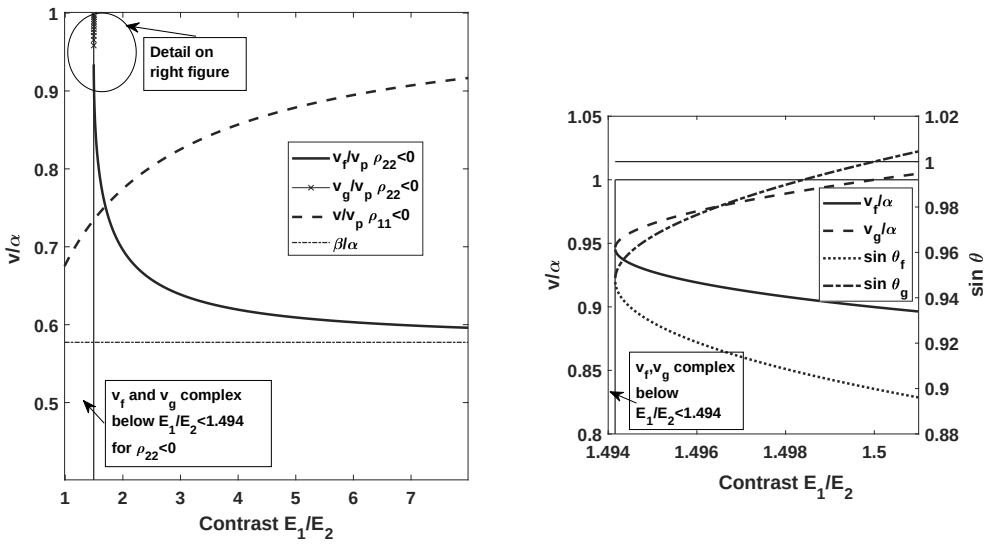

Figure 9: Wave velocities of the transmitted waves through the interface as a function of the contrast ratio. Case of S-wave incident at $\pi/4$ on the interface. The right part of the figure is a zoom on the main figure for the case $\rho_{22} < 0$ near the value of contrast below which there is no transmitted propagating wave, with addition of $sin\theta_f$ and $sin\theta_g$.

$E_0 = E_1/E_2 < E_{0s} = 1.494$, the values of r being also complex with a non-zero real part. The nature of these waves is discussed below at the end of section 5.

The interesting value E_{0s} of $E_0 = E_1/E_2$ corresponds to the case where the discriminant of equation (29) changes its sign. From the equation of the discriminant for $\nu = 1/4$, it comes:

$$E_{0s} = \frac{12a(a-1)}{(3a-1)^2} \tag{36}$$

For this contrast ratio, $v_f = v_g$ and both transmitted waves have the same wave velocity.

Above this ratio, the values of $sin(\theta)$ and wave velocity are decreasing for

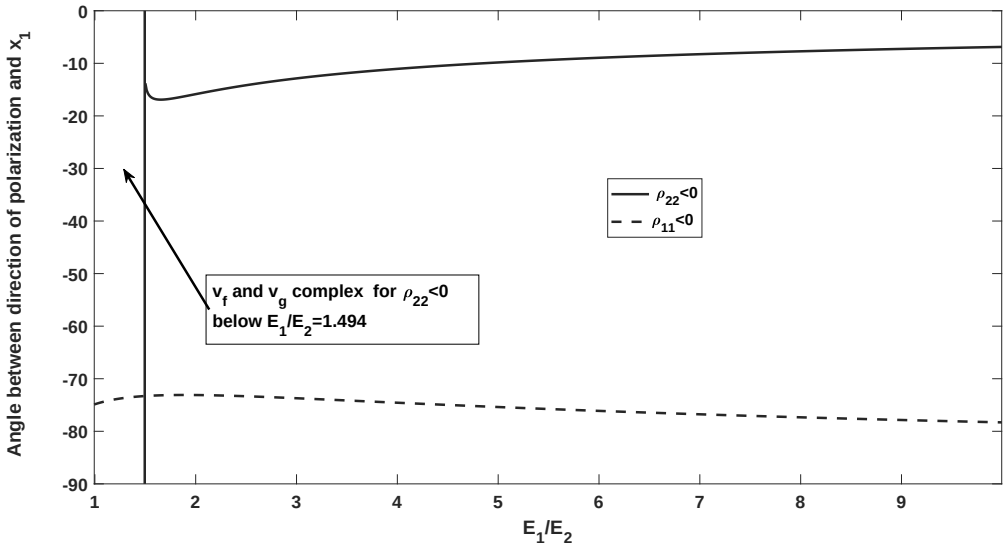

Figure 10: Angle between the direction of polarization of the main transmitted wave and $0x_1$ (two cases of dynamic density) as a function of the contrast ratio. Case of an incident S-wave. The secondary transmitted wave for $\rho_{22} < 0$ has been disregarded.

f-wave and increasing for g-wave, up to grazing refraction, i.e. $sin(\theta_g) = 1$, corresponding to $E_0 = 3/2$. For higher contrasts, $sin(\theta_g) > 1$, θ_g becomes complex and g-wave becomes e-evanescent. f-wave is still propagating with a decreasing wave velocity.

5.2.2. Polarization of transmitted waves

Figure 10 displays the direction of polarization of the transmitted waves. In the case $\rho_{22} < 0$, only the main propagating wave (f-wave) has been reported. Except in the case of lower contrast where there is no propagating waves for $\rho_{22} < 0$, the angle of polarization of propagating waves are similar to the case of incident P-wave and driven by the direction of motion corresponding to the

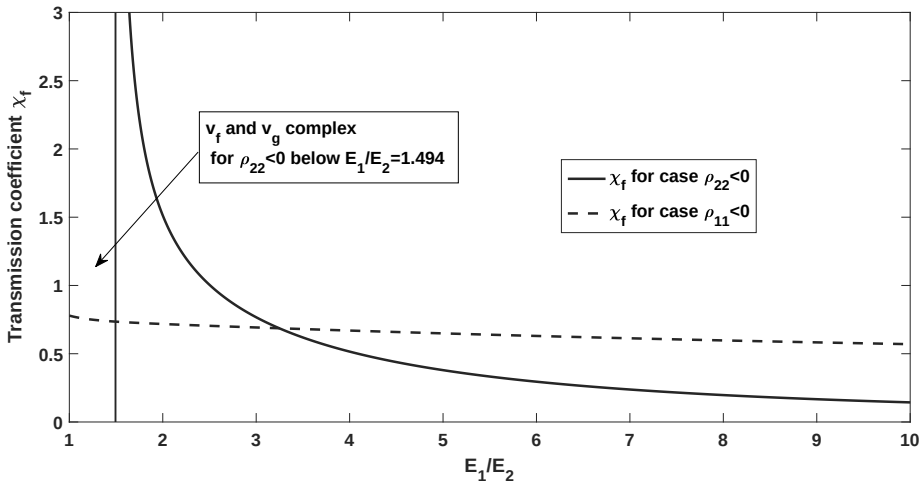

Figure 11: Ratio of the amplitudes of the Poynting vector of transmitted and incident wave (two cases of dynamic density). Case of incident S-wave. The secondary transmitted wave for $\rho_{22} < 0$ has been disregarded.

real component of dynamic density.

5.2.3. Poynting vectors and transmission coefficients.

The ratio of amplitudes of Poynting vectors is displayed on Fig.11, keeping again the main transmitted wave in the case $\rho_{22} < 0$. The features of the results are similar to the case of incident P-wave for $\rho_{11} < 0$, but differ strongly from the case of incident P-wave in the case of $\rho_{22} < 0$. Near the lower limit $E_0 = E_{0s} = 1.494$, the transmission coefficient becomes very large. It corresponds to the fact that f-wave and g-wave having the same wave velocity, matrix $[M_2]$ and $[T]$ defined in eq.(30) and (31) have two identical columns. It implies that $[T]$ is singular.

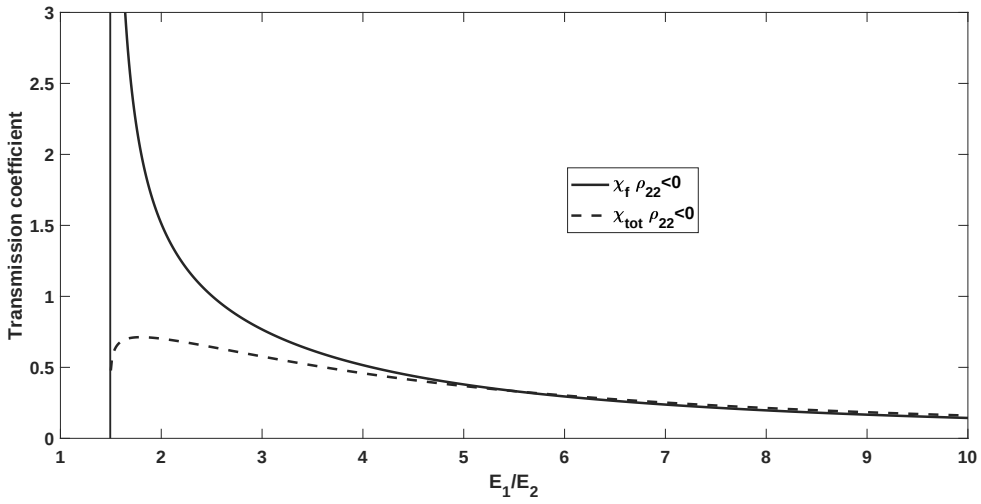

Figure 12: Ratio of the amplitudes of the Poynting vector of transmitted and incident wave (two cases of dynamic density). Case of incident S-wave for $\rho_{22} < 0$. Comparison of χ_f and χ_{tot}. The secondary transmitted wave for $\rho_{22} < 0$ has been disregarded.

It is of importance to characterize the behaviour of the reflection-refraction coefficients near this singularity. In appendix 2, it is shown that the amplitudes of the reflected waves are finite near $E_0 = E_{0s}$, but A_f behaves near this value as $A_f \sim \frac{C}{\sqrt{|p-p_s|}}$, where p_s is the slowness corresponding to $E_0 = E_{0s}$ and similarly $A_g \sim -\frac{C}{\sqrt{|p-p_s|}}$. Therefore A_f and A_g tend to $+\infty$ and $-\infty$ at $E_0 = E_{0s}$. Near the singularity, the Poynting vector of g-wave is nearly the same as the one of f-wave, because the opposite signs of A_f and A_g disappear in the expressions of the Poynting vectors that are obtained from their moduli.

This result is obviously troublesome, leading to an infinite value of transmitted energy by f-wave and g-wave. However, it can be seen that this comes from the fact that f-wave and g-wave have the same wave velocity and polarization

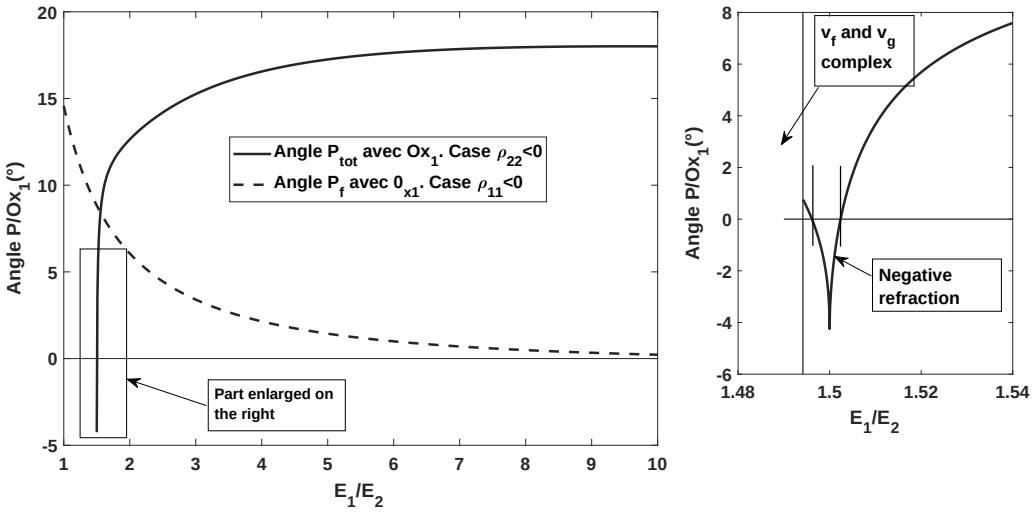

Figure 13: Case of incident S-wave. Angle between the direction of $\mathbf{P}_{tot}$ and x_2 for $\rho_{22} < 0$ and angle between the direction of $\mathbf{P}_f$ for $\rho_{11} < 0$. The right part is zooming near the singularity.

at the singularity with opposite signs of the amplitudes.

It is noticeable that replacing θ in (10) by its expression compatible with the continuity of slowness , p by p_0 and r by the double root of equation (28) produces a matrix where only one eigenvector corresponds to the common polarization, while for $p < p_0$, the matrix has two eigenvectors related to the two polarizations. This characterizes an exceptional point in the sense of Heiss (2012).

The consequence of this result is that **a strong coupling exists between f-wave and g-wave** near the singularity and that **the flux of energy must be obtained from the superposition of these waves**.

The complex Poynting vector of the coupled waves can be obtained as previ-

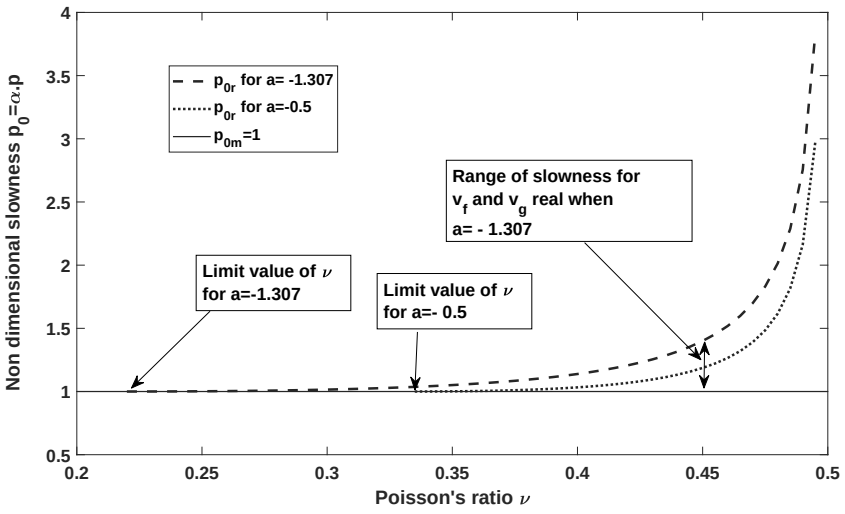

Figure 14: Non-dimensional slowness at the singularity (p_{0r}) and value p_{0m} of non-dimensional slowness when at least one wave becomes evanescent. Values of p_0 as a function of Poisson's ratio for two values of a.

ously by using the sum of stress tensors and velocities corresponding to f-wave and g-wave, leading to the total Poynting vector:

$$\begin{aligned} \mathbf{P}_{tot} &= \mathbf{P}_{ff} + \mathbf{P}_{gg} + \mathbf{P}_{fg} + \mathbf{P}_{gf} \\ \mathbf{P}_{kl} &= \frac{A_k A_l^* \omega^2}{2v_k} \left[\mathbf{\Sigma}_k\right] . \mathbf{w}_l^* \end{aligned} \tag{37}$$

where $k = f, g$, $\mathbf{w}_f = \mathbf{f}$, $\mathbf{w}_g = \mathbf{g}$

With this new notation, $\mathbf{P}_{ff} = \mathbf{P}_f$, as obtained previously. The amplitude of the real part of $\mathbf{P}_{tot}$ leads to the value of the transmission coefficient χ_{tot}.

Figure 12 shows the comparison between the values of χ_f and χ_{tot}. It appears that the flux of energy transmitted at the interface of the metamaterial given by

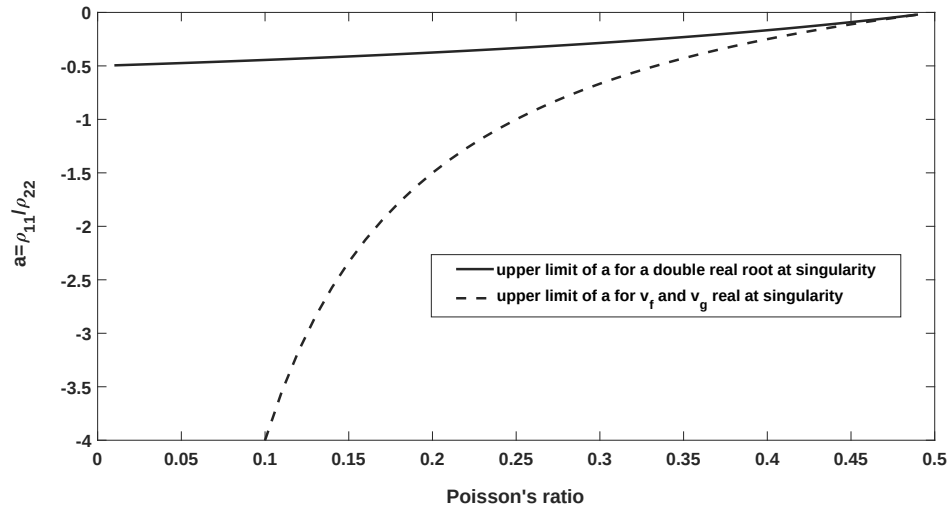

Figure 15: Upper limit of a leading to real values of r at the singularity and upper value of a (a_p) leading to propagating waves. Values of a as a function of Poisson's ratio.

χ_{tot} is now inferior to the flux of incident energy, which is physically satisfying. A last noteworthy point is that the correction provided by the coupling with g-wave is significant also in the range $3/2 < E_0 < 5$, even if g-wave is evanescent.

5.2.4. Negative refraction

As explained in the introduction, the occurrence of negative refraction in metamaterials has been the subject of numerous works. As stressed by several authors, the results on harmonic waves do not allow ones to conclude on negative refraction, but must be studied by using the group velocity. However, as shown by Auld (1973), the group velocity of bulk waves is equal to the energy velocity given by the ratio of Poynting vector to the energy density. This property has been extended in several physical situations (Laude et al., 2005; Langenberg

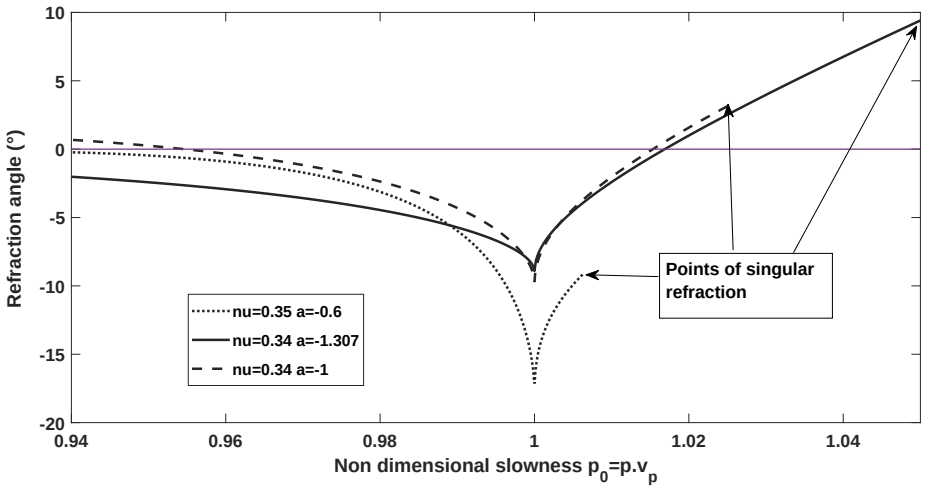

Figure 16: Inclination of the Poynting vector near the singularity as a function of non-dimensional slowness for three cases of ν, a. Case of incident S-wave for $\rho_{22} < 0$ and incidence at $\pi/4$.

et al., 2010; Nelson, 1996). So, the direction of group velocity is the same as the one of Poynting vector in all these cases. We apply this result to locally resonant materials.

The direction of Poynting vector with respect to axis Ox_2 is shown in Fig.13 for both cases of incident shear waves. It can be seen that for the case of $\rho_{11} < 0$, where the coupling between refracted waves is weak, there is only one propagating wave, the f-wave, and the Poynting vector is always oriented towards $x_1 > 0$, as for the usual refraction. The decreasing of the angle is consistent with the fact that the incident wave has an increasing wave velocity when the contrast ratio increases, this increase being higher than the increase of f-wave velocity.

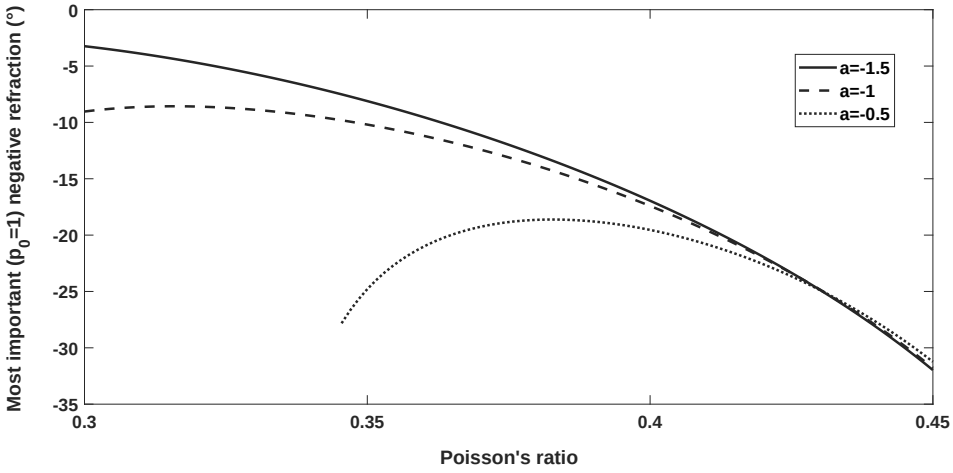

Figure 17: Inclination of the Poynting vector at its minimum ($p_0 = 1$) as a function of ν for 3 values of a. Case of incident S-wave for $\rho_{22} < 0$ and incidence at $\pi/4$.

The case of $\rho_{22} < 0$ is very different. The Poynting vector is mainly oriented towards $x_1 > 0$ and is mainly increasing with the contrast ratio, except near the singularity $E_0 = E_{0s}$. The angle of the Poynting vector with x_2 decreases from this value of E_0, up to the value of $E_0 = 3/2$ corresponding to the point where g-wave becomes evanescent. Above this value, the angle increases to reach 18° at $E_0 = 10$. The most striking point is that the Poynting vector is oriented towards $x_1 < 0$ near the singularity, implying negative refraction, for a small slot [1.496 1.502] around the minimal angle corresponding to $E_0 = 3/2$.

5.2.5. The case of two complex velocities with non-null real part

The previous results have disregarded the cases where the determinant of equation (28) is negative, leading to two complex velocities. In the case of v-

evanescent wave, the wave velocity is complex with a null real part and it is easy to provide the correct signs leading to an evanescent wave, as shown in appendix D.

For the sake of completeness, we look at the case of two complex velocities with real parts. In the case where equation (28) provides two complex and conjugate values of r, the wave velocities can be written :

$$\begin{aligned} v_f &= \pm(v_r + iv_i) \\ v_g &= \pm v_f^* = \pm(v_r - iv_i), \end{aligned}$$

where the sign of v_g is also undetermined.

The propagation of the related waves is characterized by the nature of the related slowness vectors $\mathbf{q}_f, \mathbf{q}_g$ whose components are $(q_1 = p, q_{2(f)})$ and $(q_1 = p, q_{2(g)})$ with

$$q_{2(f)} = \pm \frac{cos\theta_f}{v_f} \tag{38}$$

with an undetermined sign and similarly for $q_{2(g)}$. However, v_r and v_g being conjugate, it comes

$$q_{2(g)} = \pm q_{2(f)}^* \tag{39}$$

The choice of the signs is usually determined by these physical constraints:

- The real part q_{2r} of q_2 being positive ensures that the propagation is oriented toward $x_2 > 0$.
- The imaginary part q_{2i} of q_2 being positive ensures that the wave is attenuated for a propagation toward $x_2 > 0$.

From relation (39), it can be seen that these two conditions can not be met simultaneously for both waves, this being troublesome.

However, a result that is consistent with the physics of the system can be recovered if one computes the Poynting vectors $\mathbf{P}_f, \mathbf{P}_g, \mathbf{P}_{tot}$ in the four different cases of signs of the terms occuring in the couple q_{2f}, q_{2g}. The results show that:

- Only $\mathbf{P}_{tot}$ leads to a physically satisfying transmission coefficient ($\chi_{tot} < 1$). It means that both refracted waves are strongly coupled as it is the case near the singularity.

- Both values $q_{2(f)}, q_{2(g)}$ must be characterized by $q_{2(i)} > 0$, corresponding to an attenuation toward $x_2 > 0$.

- All other combination of signs leads to non-physical values of (χ_{tot}).

- For all cases with complex wave velocities, the real part of the component of the total Poynting vector along x_2 is null. This component becomes different from zero only when v_f and v_g become real and positive for a contrast above the singularity.

This shows that, as it is the case near the singularity, each individual wave has not in itself consistent physical properties. Only the coupled waves lead to consistent physical results and finally to no energy transmitted through the interface, like for the cases of v-evanescent and e-evanescent waves (see Appendix D).

6. The conditions leading to negative refraction

The occurrence of negative refraction near the singularity point defined previously is of prime importance and this section will now characterize the conditions to obtain this phenomenon.

Up to now, the results have been presented by using the contrast ratio $E_0 = E_1/E_2$. However, to generalize the previous results, it is thereafter preferred to use the horizontal slowness in its non-dimensional form $p_0 = p.\alpha$, where α is the wave velocity of P-wave in the metamaterial at low frequency. The relation between these variables is straightforward:

$$p_0^2 = \frac{sin^2 i_{inc}}{E_0} \left(\frac{\alpha}{v_{inc}} \right)^2 \tag{40}$$

where i_{inc} is the angle of incidence and v_{inc} the velocity of incident wave.

6.1. Condition on the orientation of the axes of dynamic density

The occurence of negative refraction is related to the occurence of a double solution of equation in r. The negative refraction is possible only if the discriminant of this equation can change its sign. It is noteworthy that this cannot be possible in the case of $\rho_{11} < 0$. As a consequence, **the negative refraction is possible only if the negative component of dynamic density corresponds to** x_2, i.e. perpendicular to the interface.

This is similar to the case of negative refraction on stratified media which appears only in the case of stratification perpendicular to the interface with the purely elastic medium (Srivastava, 2016; Willis, 2016; Mokhtari et al., 2020). Our result has therefore some similarity with these previous ones.

6.2. Value of slowness for having a double root for r.

When $\rho_{22} < 0$, equation (28) becomes

$$(1 + \frac{Lp_0^2}{2(1-\nu)})r^2 - (H+L)r + P = 0 \tag{41}$$

The singularity appears when this equation has a double root, i.e. its discriminant is null. This is achieved when

$$p_0^2 = p_{0s}^2 = \frac{((1-2\nu)(a-1)+a)^2}{4(a-1)a(1-2\nu)} \tag{42}$$

The right member of this relation is always positive. Therefore, there is always a value of p_{0s} such that the discriminant is null. The discriminant is a decreasing function of p_0 and the condition for having two real values of r is $p_0 < p_{0s}$.

6.3. Condition for two propagating waves and a singularity when $p_0 = p_{0s}$

When the discriminant is null, there are two propagating waves under two conditions.

- the value of r when $p_0 = p_{0s}$ must be positive
- the angles of refraction must be real and meet $sin(\theta_f) = sin(\theta_g) < 1$

The second condition implies the first one. The limit for the second condition is obtained when $sin(\theta_f) = 1$ combined with $p_0 = p_{0s}$. This is obtained when $a = a_p = -\frac{1-2\nu}{2\nu}$ and the condition for having two propagating waves and therefore a singularity of the transmitted waves is

$$a < -\frac{1-2\nu}{2\nu} = a_p \tag{43}$$

6.4. Condition for having two propagating waves when $p_0 < p_{0s}$.

Under the previous condition, there is a singularity and there are two propagating waves for $p_0 < p_{0s}$, just below the singularity. It can be shown that one of the values of r, chosen as the one of g-wave is increasing and the other is decreasing. The first one leads to an increasing value of wave velocity and an increasing value of $sin(\theta)$ up to reaching the grazing refraction, i.e. $sin(\theta_g) = 1$, implying $cos2\theta_g = -1$ and $sin2\theta_g = 0$. From relation (10), it can be seen that the only propagating wave corresponds to $r = b + 1$, leading to $p_0 = p_{0m} = 1$. For a lower values of p, there is one propagating wave and one evanescent wave. As a consequence, there are two propagating waves with the condition:

$$p_{0m} = 1 \leq p_0 \leq p_{0s} \tag{44}$$

6.5. The second singularity

When equation (41) has a double root, there is a singularity of transmission coefficients. There is another singularity of interest related to the values of r. Indeed, the coefficient $A = 1 + L\frac{p_0^2}{2(1-\nu)}$ of r^2 in equation (41) is null for a value of p_0 given by:

$$p_0^2 = p_{0A}^2 = 2\frac{1-\nu}{1-a} \tag{45}$$

For this value, one value of r (the one related to v_g) tends to $+\infty$ and changes its sign around this singularity. The other value of r is finite and given by:

$$r_A = \frac{4a(1-\nu)(1-2\nu)}{a + (1-2\nu)(1+a)} \tag{46}$$

For the values of p_0 inferior to p_{0A}, A becomes positive and the two values of r are of opposite signs.

In the application of section 5, the value of p_{0A} would lead to $E_0 \sim 2.3$. It can be seen on figures 11,12 that this singularity does not affect the transmission coefficients. This can be explained by the fact that v_g appears at the denominator in the expression of the part of the Poynting vector $\mathbf{P}_{tot}$ containing $\mathbf{\Sigma}_g$. This implies that the related terms are null. It is worthwhile noticing that the second singularity corresponds to the change between g-wave being e-evanescent (two positive roots of (41)) and v-evanescent (two real roots of opposite sign)).

6.6. Synthesis on the conditions leading to negative refraction

The first condition leading to a singularity is to obtain two propagating waves when $p_0 = p_{0s}$. This condition is given by the upper limit $a < a_p$. Figure 15 displays the value of a_p for different values of Poisson's ratio. It shows that this condition leads to values of $|a|$ that are large for the lowest values of Poisson's ratio, leading to smaller values of $|\rho_{22}|$, excluding the value of ρ_{22} at the center of the range of negative dynamic mass density. Keeping the previous choice of ρ_{22} implies to use materials with a Poisson's ratio larger than 0.2.

The decreasing of the angle of Poynting vector with x_2 leading to negative refraction occurs between the singularity corresponding to p_{0s} and the limit $p_{0m} = 1$ where g-wave reaches a grazing refraction. Figure 14 displays these two values, taking into account the previous limit $a = a_p$ conditioning the occurrence of two propagating waves at the singularity. It can be seen that the range $[p_{0m}, p_{0s}]$ is vanishing near 0.2 for $a = -1.307$ ($\rho_{22} = -0.765$) and near 0.3 for $a = -0.5$ ($\rho_{22} = -2$). It explains why the numerical application of the previous section for $\nu = 0.25$ led to a small range $[p_{0m}, p_{0s}]$, the Poisson's ratio being near its minimum. It is noteworthy that the lower admissible value of ν corresponds to $p_0 = p_m$. In addition, it can be shown that the tangent at the limit point is horizontal, due to $\frac{dp_{0r}}{d\nu} = 0$ when $a = a_p(\nu)$.

Finally, table 1 displays the different values of p_0 corresponding to transitions of the dynamic behaviour when the previously described conditions are met. Obtaining all these transitions is possible only if the condition involving a_p described in figure 15 is met. In addition, figure 18 displays the different kinds

of f-wave and g-wave that are refracted within the metamaterial according to the value of the horizontal slowness.

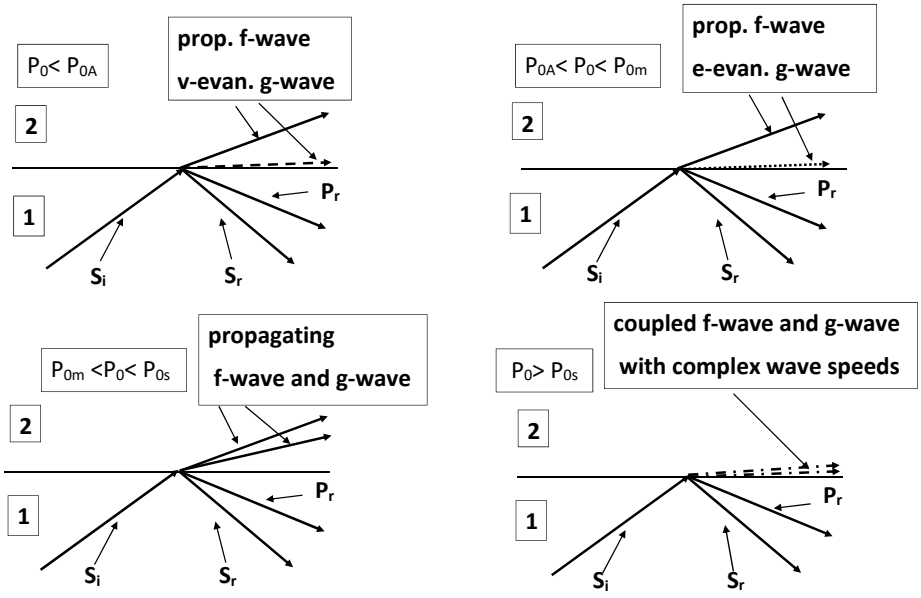

Figure 18: The different kinds of waves appearing in the metamaterial according to the value of non-dimensional horizontal slowness p_0.

These results provide necessary conditions to obtain negative refraction. Figure 16 displays the results corresponding to three kinds of materials where negative refraction is significant. It can be seen that refraction angles decrease from the points of singular refraction and are all minimum for $p_0 = 1$ when g-wave reaches the grazing refraction. For two of these examples, the angle of refraction is positive at the point of singular refraction and decreases to reach negative values at $p_0 = 1$, but for the third case, the angle of refraction is already negative at $p_0 = p_{0s}$ leading to the largest negative refraction, with an angle of refraction reaching 18°. Finally, figure 17 displays the most effective

$p_0 < p_{0A}$	$p_{0A} < p_0 < p_{0m}$	$p_{0m} < p_0 < p_{0s}$	$p_0 = p_{0s}$	$p_{0s} < p_0$
v_f real	v_f real	v_f real	$v_g = v_f$	v_f complex.
v_g imag.	v_g real	v_g real	$v_g = v_f$	v_g complex.
f prop.	f prop.	f prop.	f wave=g wave	f and g coupled
g v-evan.	g e-evan.	g prop.	f wave=g wave	f and g coupled

Table 1: The values of non-dimensional slowness p_0 leading to transitions of the dynamic behaviour. Notice that when f and g are coupled with complex wave velocities (right column), there is no energy transmitted into the metamaterial. The case $p_0 = p_{0s}$ corresponds to the exceptional point.

negative refraction (i.e. the one related to $p_0 = 1$) as a function of ν for three values of negative dynamic density characterized by a. It shows that negative refraction is larger for $a = -0.5$, i.e. when $|\rho_{22}|$ is higher. However, it can be seen that using $a = -0.5$ is possible only for a lower range of Poisson's ratios, due to the condition coming from figure (15). These results provide the means to design materials with a significant negative refraction.

7. Conclusion

The propagation of waves in a locally resonant metamaterial with an anisotropic dynamic density has been studied. The dynamic density is a second order tensor that is diagonal in axes corresponding to the symmetries of the resonant inclusion. For directions of propagation in a plane with polarization in the same plane, two of the components of dynamic density are concerned. The material has been studied when one component of dynamic mass density is negative and the other one is equal to the static mass density. The plane propagation in an infinite metamaterial has been characterized by using an extended Christoffel matrix. It has been shown that along one direction, two kinds of waves are obtained: one is propagating and the other is evanescent in the frequency range of negative mass density. The first one is dispersive except for the directions of propagation along the symmetry axes of the resonant inclusions. The second wave propagates outside the range of negative mass density and the phase

velocity tends to infinity near the upper bound of negative mass density. The polarization angles of both waves are not parallel or perpendicular to the direction of propagation except for the propagation along the axes of symmetry of resonant inclusions.

The second part of this work deals with the refraction of waves at the interface between a metamaterial with anisotropic density and an elastic material. Both materials have the same Poisson's ratio, but different elastic moduli. The orientation corresponding to a negative component of mass density governs the pattern of refracted waves. When the direction related to the negative component of dynamic mass density is parallel to the interface between elastic material and metamaterial, only one wave is propagating through the metamaterial (limited by grazing refraction), the other one being evanescent. On the contrary, when this direction is perpendicular to the interface, there are zero, one or two propagating waves, depending on the horizontal slowness of the incident wave and on the components of dynamic density in the metamaterial.

The most interesting, from a physical point of view, occurs for the horizontal slowness corresponding to the transition between zero and two propagating waves. At this point, the two propagating waves have the same wave velocity. In this case, the system giving the transmission coefficients at the interface is singular. It has been shown that the Poynting vector of each of the propagating waves is singular, and that the energy flux must be obtained by accounting simultaneously for both waves, due to a strong coupling between these waves at the singularity. It leads to a finite combined Poynting vector. Finally, it has been shown that the angle of Poynting vector with the normal to the interface decreases near the singularity and can become negative, i.e. negative refraction can occur. The parameters of the metamaterial restricting the possibility of negative refraction are characterized and several examples of negative refraction are shown.

The extension of this work to more general situations, like materials having elastic anisotropy or waves coming from fluids instead of elastic solids,... will not imply strong modifications. Indeed, all important results come from the main

equation giving the metamaterial wave velocities consistent with the horizontal slowness of incoming wave (fluid or solid) and the polarization of the related waves, all coming from an extended Christoffel matrix that can be built easily even in the case of elastic anisotropy of the metamaterial.

8. Appendix A: Group velocity of waves

8.1. Case of shear waves propagating along x_1 above the frequency bandgap

The group velocity is given from the frequency dependent phase velocity $v(\omega)$ by the usual formula $v_g = \frac{v}{1-\omega v'/v}$ where $v' = \frac{dv}{d\omega}$. This leads to

$$v_g = \beta \frac{(\omega^{*2}-1)^{3/2}(\omega^{*2}(1-d\rho^*)-1)}{1+\omega^{*2}(1-d\rho^*)(\omega^{*2}-2)} \tag{47}$$

where β is the shear wave velocity at low frequency. Similar expressions can be obtained for frequencies lower than ω_r

8.2. Case of waves propagating along any direction

The solution for r related to the propagating wave is given by:

$$r = \frac{T+\sqrt{\Delta}}{2} \tag{48}$$

with

$$\Delta = T^2 - 4P \tag{49}$$

where $T = b(1+a) + \cos 2\theta(a-1)$ and $P = a(b^2-1)$. The derivative of r with respect to ω^* is given by:

$$r' = \frac{a'}{2}(T_{,a} + \frac{\Delta_{,a}}{2\sqrt{\Delta}}) \tag{50}$$

where

$$\Delta_{,a} = -2b^2 + 2b^2a + 4ab\cos 2\theta + 2a\cos^2 2\theta - 2\cos^2 2\theta + 4 \tag{51}$$

and

$$T_{,a} = b + \cos 2\theta \tag{52}$$

The expression of a' gives:

$$a' = \frac{da}{d\omega^*} - \frac{2\omega^* d\rho^*}{(1+(d\rho^*-1)\omega^{*2})^2} \tag{53}$$

The group velocity v_g is given by :

$$v_g = \frac{v}{1-\omega^* v'/v} \tag{54}$$

where the phase velocity is

$$v = A\sqrt{r}, \tag{55}$$

A being a constant.

$$\frac{v'}{v} = \frac{r'}{2r} \tag{56}$$

Finally, the group velocity is given by :

$$v_g = \frac{v}{1-\omega^* r'/2r} \tag{57}$$

9. Appendix B: Reflexion-transmission coefficients at the singularity when f=g

The system of equations giving the transmission coefficients can be written:

$$[T] \begin{bmatrix} A_{rp} \\ A_{rs} \\ A_f \\ A_g \end{bmatrix} = [B]$$

Matrix $[T]$ can be decomposed using its column vectors

$$[T] = \begin{bmatrix} [K] & [L] & [M] & [N] \end{bmatrix}$$

For $\mathbf{f} = \mathbf{g}$, $\theta_f = \theta_g, v_f = v_g$, corresponding to the value of the slowness p_s, the third and fourth columns are identical

$$[M(p_s)] = [N(p_s)] = [M_0]$$

As a consequence, the determinant $|T(p_s)|$ of $[T(p_s)]$ is null and this matrix is singular. The behaviour of $r(p)$ at the vicinity of p_s is characterized by $r(p) - r(p_s) \sim \sqrt{|p - p_s|}$, leading to $[M] = \left[M_0 + M'.\sqrt{|p - p_s|}\right]$ and similarly for $[N]$

The value of A_{rp} at first order is obtained from the determinants:

$$A_{rp} = \frac{\begin{vmatrix} [B] & [L] & [M'] & [M_0] \end{vmatrix} + \begin{vmatrix} [B] & [L] & [M_0] & [N'] \end{vmatrix}}{\begin{vmatrix} [K] & [L] & [M'] & [M_0] \end{vmatrix} + \begin{vmatrix} [K] & [L] & [M_0] & [N'] \end{vmatrix}}$$

and similarly for A_{rs}

The values of A_f and A_g at the leading order are given by:

$$A_f \sim \frac{\begin{vmatrix} [K] & [L] & [B] & [M_0] \end{vmatrix}}{\sqrt{|p - p_s|}(\begin{vmatrix} [K] & [L] & [M'] & [M_0] \end{vmatrix} + \begin{vmatrix} [K] & [l] & [M_0] & [N'] \end{vmatrix})} \sim -A_g$$

From these expressions, it can be seen that A_{rp} and A_{rs} are finite around $p = p_s$, while A_f and A_g behave as

$$A_f \sim -A_g \sim \frac{C}{\sqrt{|p - p_s|}}$$

10. Appendix C: Effect of group velocity on time average Poynting vector

An important feature of the waves through the metamaterial is that they are dispersive, as shown in section 3. As a consequence, the group velocity is not equal to the phase velocity. This may have a consequence on the average Poynting vector transmitted through the metamaterial. To clarify this point, it is necessary to take into account that a signal of finite duration is transmitted to the material. Brillouin (1960) considers a signal $f(t)$ such that

$$f(t) = \sin \omega_0 t.\Pi(t)$$

where $\Pi(t)$ is the gate function: $\Pi(t) = 1$ for t between 0 et T and null elsewhere.

Brillouin (1960) shows that the plane wave of unit propagation vector $\mathbf{p}$, phase velocity v_0 at $\omega = \omega_0$, group velocity v_g at ω, and such that $\mathbf{u}(0,\mathbf{t}) = \mathbf{u_0} f(t)$ has a displacement given by:

$$\begin{aligned}\mathbf{u}(\mathbf{x},t) &= \mathbf{u}_0 \,\mathrm{Re}\left\{ e^{i\omega_0(\frac{\mathbf{p}.\mathbf{x}}{v_0}-t)} \int_{\omega_0-\eta}^{\omega_0+\eta} \frac{1}{2\pi} \left[e^{i\Delta\omega(\frac{\mathbf{p}.\mathbf{x}}{v_g}-t+T)} - e^{i\Delta\omega(\frac{\mathbf{p}.\mathbf{x}}{v_g}-t)} \right] \frac{d\omega}{\omega-\omega_0} \right\} \\ &= \mathbf{u}_0 \,\mathrm{Re}\left\{ e^{i\omega_0(\frac{\mathbf{p}.\mathbf{x}}{v_0}-t)} \int_{\omega_0-\eta}^{\omega_0+\eta} F(\omega,\mathbf{x},t)d\omega \right\} = \mathbf{u}_0 \,\mathrm{Re}\left\{ e^{i\omega_0(\frac{\mathbf{p}.\mathbf{x}}{v_0}-t)} M(\mathbf{x},t) \right\}\end{aligned}$$

where $\Delta\omega = \omega - \omega_0$. Function $M(\mathbf{x},t)$ corresponds to a low frequency modulation of the purely harmonic function

$$\mathbf{u}_h(\mathbf{x},t) = \mathbf{u}_0 \,\mathrm{Re}\left\{ e^{i\omega_0(\frac{\mathbf{p}.\mathbf{x}}{v_0}-t)} \right\}$$

If T is large compared with the period $T_0 = \frac{2\pi}{\omega_0}$, the frequency spectrum of $M(\mathbf{x},t)$ contains frequencies that are small compared to ω_0. As a consequence, the wave vectors related to these frequency components are small compared to the main wave vector $\frac{\omega_0 \mathbf{p}}{v_0}$ in $\mathbf{u}_h$. It follows that the stress tensor at point $\mathbf{x} = 0$ can be approximated by:

$$\sigma(\mathbf{x}=0,t) = \sigma_h(\mathbf{x}=0,t).M(\mathbf{x}=0,t)$$

where σ_h is the stress tensor computed from $\mathbf{u}_h$. From the definition of $\mathbf{u}(0,\mathbf{t})$, it comes

$$M(\mathbf{x}=0,t) = \Pi(t)$$

and the instantaneous Poynting vector is :

$$\begin{aligned}\mathbf{P}(t) &= \sigma_h(\mathbf{x}=0,t).\mathbf{u}_h(\mathbf{x}=0,t).\Pi^2(t) \\ &= \sigma_h(\mathbf{x}=0,t).\mathbf{u}_h(\mathbf{x}=0,t).\Pi(t)\end{aligned}$$

Its time average is obviously the same as the average $\bar{\mathbf{P}}_0$ over one period, given by:

$$\bar{\mathbf{P}}_0 = \frac{1}{T_0}\int_0^{T_0} \sigma_h(t, \mathbf{x}=0).\mathbf{u}_h(t, \mathbf{x}=0)dt$$

690 However, in the case of a short transient signal, it would be necessary to take into account the full spectrum of $\mathbf{u}(\mathbf{x}, \mathbf{t})$. This would imply to take into account the group velocity, which appears in the Fourier expansion of $\mathbf{u}(\mathbf{x},t)$.

11. Appendix D: Evanescent waves and complex velocities.

11.1. Refraction beyond grazing refraction: e-evanescent wave

Evanescent waves are well known in the case of classical reflection/refraction of elastic waves. The reflexion between horizontal slownesses writes:

$$\frac{sin\theta_f}{V_f} = p \tag{58}$$

where p is given by the inclination and velocity of incident wave. V_f is the wave velocity of refracted wave and θ_f the refraction angle. Beyond grazing refraction, $V_f.p > 1$ and the sinus of the refaction angle is larger than 1, its cosinus being purely imaginary. In this case, the wave field reads:

$$\mathbf{u}_f = A_f.\mathbf{f}exp(i\omega.p.x_1 - t)exp(-\omega.x_2\frac{\sqrt{p^2V_f^2 - 1}}{V_f}) \tag{59}$$

695 The penetration length of the evanescent wave is $\Lambda = \frac{V_f}{\omega\sqrt{p^2V_f^2-1}}$. This case corresponds to the usual case of evanescent waves in elasticity. Hence the name e-evanescent waves. This case appears when equation (28) provides two positive values of r and therefore two real velocities: in this case, g-wave can become evanescent in the usual sense.

700 *11.2. Case of an imaginary velocity: v-evanescent wave*

When one of the values of r is negative, for example r_g, v_g becomes purely imaginary, with $v_g = i|v_g|$. In this case, the wave field reads:

$$\mathbf{u}_g = A_g.\mathbf{g}exp(i\omega.p.x_1 - t)exp(-\omega x_2\frac{\sqrt{1 + p^2|v_g|^2}}{|v_g|}) \tag{60}$$

The penetration length becomes $\Lambda = \frac{|v_g|}{\omega\sqrt{1+p^2|v_g|^2}}$. This occurs in section 3 when one of the values of r given by the extended Christoffel matrix is negative and in section 4 when equation (28) provides one or two real and negative values of r. In this case, the evanescent wave is due to the purely imaginary nature of v_f. Hence, the name v-evanescent wave.

It is worthwhile noticing that in both cases of evanescent waves, the vertical component of the Poynting vector is null: there is no transfer of energy through the interface.

11.3. Case of two complex wave velocities

In the case where equation (28) provides two complex and conjugate values of r with non-null real parts, the situation is more intricate and the set of waves is characterized by a strong coupling and also by no transfer of energy through the interface. This is discussed at the end of section 5.

References

Akl, W., Esabbagh, A., & Baz, A. (2012). Acoustic metamaterials with circular sector cavities and programmable densities. *Journal of the Acoustical Society of America*, *132*, 2857–2865.

Auld, B. (1973). *Acoustic fields and waves in solids*. New York: Wiley.

Auriault, J. (1994). Acoustics of heterogeneous media: macroscopic behavior by homogenization. *Current Topics in Acoustical Research*, *1*, 63–90.

Auriault, J., & Bonnet, G. (1985). Dynamique des composites élastiques périodiques. (Dynamics of periodic elastic composites). *Arch. Mech.*, *37*, 269–284.

Auriault, J., & Boutin, C. (2012). Long wavelength inner-resonance cut-off frequencies in elastic composite materials. *International Journal of Solids and Structures*, *49*, 3269–3281.

Baz, A. (2010). An active acoustic metamaterial with tunable effective density. *ASME Journal of Vibration and Acoustics*, *132*, 0410111–0410119.

Bigoni, D., Guenneau, S., Movchan, A. B., & Brun, M. (2013). Elastic metamaterials with inertial locally resonant structures: Application to lensing and localization. *Physical Review B*, *84*, 174303.

Bonnet, G., & Monchiet, V. (2015). Low frequency locally resonant metamaterials containing composite inclusions. *Journal of the Acoustical Society of America*, *137*, 3263–3271.

Bonnet, G., & Monchiet, V. (2017). Dynamic mass density of resonant metamaterials with homogeneous inclusions. *Journal of the Acoustical Society of America*, *142*, 890–901.

Bonnet, G., & Monchiet, V. (2020). Dynamic behaviour of elastic metamaterials containing soft elliptic fibers. *Journal of the Mechanics and Physics of Solids*, *140*, 103953.

Boutin, C., Auriault, J., & Bonnet, G. (2018). Inner resonance in media governed by hyperbolic and parabolic dynamic equations. Principle and examples. In H. Altenbach, J. Pouget, M. Rousseau, B. Collet, & T. Michelitsch (Eds.), *Generalized Models and Non-classical Approaches in Complex Materials.* chapter 6. (pp. 83–84). Berlin: Springer.

Brillouin, L. (1960). *Wave propagation and group velocity*. Cambridge, Massachusets: Academic Press.

Brunet, T., Merlin, A., Mascaro, B., Zimny, K., Leng, J., Poncelet, O., Aristégui, C., & Mondain-Monval, O. (2015). Soft 3D acoustic metamaterial with negative index. *Nature Materials*, *14*, 384–388.

Christensen, J., & García De Abajo, F. J. (2012). Anisotropic metamaterials for full control of acoustic waves. *Physical Review Letters*, *108*, 124301.

Christiansen, R., & Sigmund, O. (2016). Experimental validation of systematically designed acoustic hyperbolic meta material slab exhibiting negative refraction. *Applied Physics Letters*, *109*, 101905.

Eringen, A., & Suhubi, E. (1978). *Elastodynamics,Vol.2.*. N.Y.: Acad. Press.

Han, J., Wen, T., Yang, P., & Zhang, L. (2014). Negative refraction imaging of acoustic metamaterial lens in the supersonic range. *AIP Advances*, *4*, 057126.

Heiss, W. (2012). The physics of exceptional points. *J. Phys. A: Math. Theor.*, *45*, 444016.

Hladky-Hennion, A. ., Vasseur, J. O., Haw, G., Croënne, C., Haumesser, L., & Norris, A. N. (2013). Negative refraction of acoustic waves using a foam-like metallic structure. *Applied Physics Letters*, *102*.

Huang, H., & Sun, C. (2011). Locally resonant acoustic metamaterials with 2D anisotropic effective mass density. *Philosophical Magazine*, *91*, 981–996.

Huang, H., & Sun, C. (2012). Anomalous wave propagation in a one-dimensional acoustic metamaterial having simultaneously negative mass density and Young's modulus. *Journal of the Acoustical Society of America*, *132*, 2887–2895.

Kaina, N., Lemoult, F., Fink, M., & Lerosey, G. (2015). Negative refractive index and acoustic superlens from multiple scattering in single negative metamaterials. *Nature*, *525*, 77–81.

Krushynska, A., Bosia, F., Miniaci, M., & Pugno, N. (2017). Spider web-structured labyrinthine acoustic metamaterials for low-frequency sound control. *New Journal of Physics*, *19*, 105001.

Langenberg, K. J., Marklein, R., & Mayer, K. (2010). Energy vs. group velocity for elastic waves in homogeneous anisotropic solid media. In *Symposium Digest - 20th URSI International Symposium on Electromagnetic Theory, EMTS 2010* (pp. 733–736).

Laude, V., Reinhardt, A., & Khelif, A. (2005). Equality of the energy and group velocities of bulk acoustic waves in piezoelectric media. *IEEE transaction on ultrasonics, ferroelectrics and frequency control*, *52*, 1869–1871.

Lee, S., Park, C., Seo, Y., Wang, Z., & Kim, C. (2009). Acoustic metamaterial with negative density. *Physical letters A*, *373*, 4464–4469.

Lemoult, F., Kaina, N., Fink, M., & Lerosey, G. (2013). Wave propagation control at the deep subwavelength scale in metamaterials. *Nature Physics*, *9*, 55–60.

Liu, J., Guo, H., & Wang, T. (2020). A review of acoustic metamaterials and phononic crystals. *Crystals*, *10*, 305.

Liu, Z., Zhang, X., Mao, Y., Zhu, Y., Yang, Z., Chan, C., & Sheng, P. (2000). Locally resonant materials. *Science*, *289*, 1734–1736.

Ma, G., & Sheng, P. (2016). Acoustic metamaterials: From local resonances to broad horizons. *Science Advances*, *2*, e1501595.

Milton, G. (2007). New metamaterials with macroscopic behavior outside that of continuum elastodynamics. *New Journal of Physics*, *9*, 359.

Milton, G., & Willis, J. (2007). On modifications of Newton's second law and linear continuum elastodynamics. *Proceedings of the Royal Society A*, *463*, 855–880.

Mokhtari, A. A., Lu, Y., Zhou, Q., Amirkhizi, A. V., & Srivastava, A. (2020). Scattering of in-plane elastic waves at metamaterial interfaces. *International Journal of Engineering Science*, *150*, 103278.

Naify, C., Chang, C., Mcknight, G., & Nutt, S. (2012). Scaling of membrane-type locally resonant acoustic metamaterial arrays. *Journal of the Acoustical Society of America*, *132*, 2784–2792.

Nassar, H., He, Q., & Auffray, N. (2015). Willis elastodynamic homogenization theory revisited for periodic media. *Journal of the Mechanics and Physics of Solids*, *77*, 158–178.

Nassar, H., He, Q., & Auffray, N. (2016). On asymptotic elastodynamic homogenization approaches for periodic media. *Journal of the Mechanics and Physics of Solids*, *88*, 274–290.

Nelson, D. (1996). Generalizing the Poynting vector. *Physical Review Letters*, *76*, 4713–4716.

Park, J., Park, B., Kim, D., & Park, J. (2012). Determination of effective mass density and modulus for resonant metamaterials. *Journal of the Acoustical Society of America*, *132*, 2793–2799.

Sheng, P., Zhang, X., Liu, Z., & Chan, C. (2003). Locally resonant sonic materials. *Physica B*, *338*, 201–205.

Srivastava, A. (2016). Metamaterial properties of periodic laminates. *Journal of the Mechanics and Physics of Solids*, *96*, 252–263.

Veselago, V. (1968). The electrodynamics of substances with simultaneously negative values of ϵ and μ. *Soviet Physics Uspekhi*, *10*, 509–514.

Willis, J. (1981). Variational principles for dynamic problems for inhomogeneous elastic media. *Wave Motion*, *3*, 1–11.

Willis, J. (2016). Negative refraction in a laminate. *Journal of the Mechanics and Physics of Solids*, *97*, 10–18.

Wu, J., Wang, X., Tang, B., He, Z., Deng, K., & Zhao, H. (2017). Elastic metamaterial with simultaneously negative refraction for longitudinal and transverse waves. *AIP Advances*, *7*, 105309.

Xie, Y., Popa, B.-I., Zigoneanu, L., & Cummer, S. (2013). Measurement of a broadband negative index with space-coiling acoustic metamaterials. *Physical Review Letters*, *110*, 175501.

Yang, Z., Mei, J., Yang, M., Zhou, N. C., & Sheng, P. (2008). Membrane-type acoustic metamaterial with negative dynamic mass. *Physical Review Letters*, *101*, 204301.

Yao, S., Zhou, X., & Hu, G. (2008). Experimental study on negative effective mass in a 1D mass-spring system. *New Journal of Physics*, *10*, 043020.

Zhang, X., & Liu, Z. (2004). Negative refraction of acoustic waves in two-dimensional phononic crystals. *Applied Physics Letters*, *85*, 341–343.

Zhou, X., Liu, X., & Huc, G. (2012). Elastic metamaterials with local resonances: an overview. *Theoretical and applied mechanics letters*, *2*, 041001.

Zhu, R., Liu, X. N., Hu, G. K., Sun, C. T., & Huang, G. L. (2014). Negative refraction of elastic waves at the deep-subwavelength scale in a single-phase metamaterial. *Nature Communications*, *5*, 5510.